

Exact ZF Analysis and Computer-Algebra-Aided Evaluation in Rank-1 LoS Rician Fading

Constantin Siriteanu, Akimichi Takemura, Christoph Koutschan,
Satoshi Kuriki, Donald St. P. Richards, Hyundong Shin

Abstract

We study zero-forcing detection (ZF) for multiple-input/multiple-output (MIMO) spatial multiplexing under transmit-correlated Rician fading for an $N_R \times N_T$ channel matrix with rank-1 line-of-sight (LoS) component. By using matrix transformations and multivariate statistics, our exact analysis yields the signal-to-noise ratio moment generating function (m.g.f.) as an infinite series of gamma distribution m.g.f.'s and analogous series for ZF performance measures, e.g., outage probability and ergodic capacity. However, their numerical convergence is inherently problematic with increasing Rician K -factor, N_R , and N_T . We circumvent this limitation as follows. First, we derive differential equations satisfied by the performance measures with a novel automated approach employing a computer-algebra tool which implements Gröbner basis computation and creative telescoping. These differential equations are then solved with the holonomic gradient method (HGM) from initial conditions computed with the infinite series. We demonstrate that HGM yields more reliable performance evaluation than by infinite series alone and more expeditious than by simulation, for realistic values of K , and even for N_R and N_T

C. Siriteanu is with the Graduate School of Information Science and Technology, Osaka University, Japan.

A. Takemura is now with the Center for Data Science Education and Research, Shiga University, Hikone, Japan. Until March 2016, he was with the Graduate School of Information Science and Technology, University of Tokyo, Japan. A. Takemura acknowledges the Japan Society for the Promotion of Science Grant-in-Aid for Scientific Research No. 25220001.

C. Koutschan is with the Johann Radon Institute for Computational and Applied Mathematics, Austrian Academy of Sciences, Linz, Austria. The work of C. Koutschan was supported by the Austrian Science Fund (FWF): DK W1214.

S. Kuriki is with the Institute of Statistical Mathematics, Tachikawa, Tokyo, Japan.

D. St. P. Richards is with the Department of Statistics, Pennsylvania State University, University Park, PA, USA.

H. Shin is with the Department of Electronics and Radio Engineering, Kyung Hee University, South Korea. The work of H. Shin was supported by the National Research Foundation of Korea through the Ministry of Science, ICT, and Future Planning, under Grant 2013-R1A1A2-019963.

relevant to large MIMO systems. We envision extending the proposed approaches for exact analysis and reliable evaluation to more general Rician fading and other transceiver methods.

Index Terms

Computer algebra, holonomic gradient method, Rician (Ricean) fading, MIMO, zero-forcing detection.

I. INTRODUCTION

A. Background, Motivation, and Scope

The performance of multiple-input/multiple-output (MIMO) wireless communications systems has remained under research focus as the multiantenna architectures that attempt to harvest MIMO gains have continued to evolve, e.g., from single-user MIMO, to multi-user and distributed MIMO, and, most recently, to massive or large MIMO [1], [2], [3], [4], [5], [6], [7].

As the numbers of transmitting and receiving antennas, herein denoted with N_T and N_R , respectively, have increased in seeking higher array, diversity, and multiplexing gains [1, pp. 72, 64, 385], transceiver processing complexity has also increased. For spatial multiplexing transmission, linear detection methods [3], [5], [6], e.g., zero-forcing detection (ZF) and minimum mean-squared-error detection (MMSE), are attractive because of their relatively-low complexity order $\mathcal{O}(N_R N_T + N_R N_T^2 + N_T^3)$ [6] and their good performance for $N_R \gg N_T$, as the columns of the $N_R \times N_T$ channel matrix \mathbf{H} tend to become independent [6].

For increased practical relevance, MIMO channel model complexity has also been growing, and, with it, the difficulties of MIMO performance analysis and numerical evaluation. Thus, early ZF research assumed zero-mean, i.e., Rayleigh fading, for the elements of \mathbf{H} , which enabled relatively simple analysis and evaluation [8], [9], [10]. Recently, various cases of nonzero-mean \mathbf{H} , i.e., Rician fading, have rendered increasingly more difficult the analysis and evaluation for several transceiver methods [11], [12], [13], [14], [15], [16], [17], [18], [19], [20], [21].

Rician fading can occur due to line-of-sight (LoS) propagation, in indoor, urban, and suburban scenarios, as shown by the WINNER II channel measurements [22, Section 2.3]. WINNER II [22, Table 5.5] has also characterized as lognormal the distributions of 1) the Rician K -factor, which determines the strength of the channel mean vs. standard deviation [1, p. 37], and 2) the azimuth spread (AS), which determines the antenna correlation [23, p. 136]. An ability to

evaluate MIMO performance over the range of realistic values of K and AS is useful, e.g., in averaging over their distributions, which has only rarely been attempted before [18].

Consequently, we focus herein on evaluating MIMO ZF under transmit-correlated Rician fading. For tractable analysis we assume as in [15], [16] that the LoS or deterministic component of \mathbf{H} satisfies $\text{rank}(\mathbf{H}_d) = r = 1$. Whereas for LoS propagation r can take any value from 1 to N_T [24], [25], [26], [27], small antenna apertures, relatively-low carrier frequency, or large transmitter-receiver distance, as in conventional point-to-point deployments [1], [16], are likely to yield \mathbf{H}_d as outer product of array response vectors [1, Eq. (7.29), p. 299], i.e., $r = 1$.

Our future work shall consider Rician fading with $r > 1$ for ZF and MMSE. Higher r , which improves \mathbf{H} conditioning, i.e., MIMO performance, is becoming increasingly more relevant due to envisioned LoS millimeter-wave applications [24]. MMSE is appealing because it outperforms ZF. Also, we shall tackle more general statistical fading models that can characterize more modern MIMO deployment types [17]. Finally, for millimeter waves and massive MIMO, we shall pursue beamspace channel matrix representation and signal processing [27], [25], [28].

B. Limitations of Relevant Previous Work on MIMO ZF

Historically, the study of MIMO ZF commenced with that for uncorrelated Rayleigh fading from [8]. The case of transmit-correlated Rayleigh fading was elucidated in [9], [10]. For Rician fading, previous studies assumed certain values for r and/or proceeded by approximation:

- Rician fading only for 1) the intended stream, i.e., *Rician-Rayleigh fading*, which is a special case with $r = 1$, or 2) the interfering streams, i.e., *Rayleigh-Rician fading*, whereby $r = N_T - 1$; these cases may arise in heterogeneous networks. Then, we derived in [19] exact infinite-series expressions for performance measures, e.g., the average error probability, outage probability, and ergodic capacity (i.e., rate [15], [17]) — more details below.
- Rician fading for all streams, i.e., *full-Rician fading*, for the special case with $r = 1$. Early works — see [18], [29] and references therein — used an approximation of the cumbersome noncentral-Wishart distribution of $\mathbf{H}^H \mathbf{H}$ with a central-Wishart distribution of equal mean, which has yielded a simple gamma distribution for the signal-to-noise ratio (SNR). Then, [18], [21] reveal that $r = 1$ does not ensure consistent accuracy¹ and $r > 1$ can render it

¹Only very careful usage in [18] helped average the performance over WINNER II distributions of K and AS for $r = 1$.

useless. Recently, bounding techniques have yielded — only for uncorrelated fading — the simple sum rate bounds in [15, Eqs. (55)–(58)] that become accurate at high SNR.

- Rician fading, $\forall r = 1, \dots, N_T$. For this most general case, exact sum-rate expressions for $N_R \rightarrow \infty$ and approximations for finite N_R were derived in [17].

For Rician–Rayleigh fading, we have recently analyzed and evaluated ZF exactly in [19], [20]. In [19], we expressed the SNR moment generating function (m.g.f.) in terms of the confluent hypergeometric function ${}_1F_1(\cdot, \cdot, \sigma)$ [19, Eq. (31)], where $\sigma \propto KN_R N_T$. Thereafter, its well-known expansion around $\sigma_0 = 0$ [19, Eq. (30)] yielded an infinite series of gamma distribution m.g.f.’s [19, Eq. (37)]. Finally, inverse-Laplace transformation and integration yielded analogous series for the SNR probability density function (p.d.f.), average error probability, outage probability, and ergodic capacity [19, Eqs. (39), (58), (69), (71)]. However, beside complicating the analysis, the Wishart distribution noncentrality induced by Rician fading also leads to numerical divergence for these series with increasing K , N_R , and N_T [19, Section V.F]. In [20], we overcame this limitation by using the fact that ${}_1F_1(\cdot, \cdot, \sigma)$ is a *holonomic function*², i.e., it satisfies a differential equation [20, Eq. (27)] with polynomial coefficients with respect to (w.r.t.) σ . Starting from this differential equation, a difficult by-hand derivation produced differential equations for the SNR m.g.f. and then for the SNR p.d.f., via inverse-Laplace transform. Thereafter, we computed reliably the p.d.f. at realistic values of K — but only for relatively small N_R and N_T — by numerically solving its differential equations from initial conditions computed with the infinite series for small K . This approach is known as the *holonomic gradient method* (HGM) because, at each step, the function value is updated with the differential gradient [20, Sec. IV.B]. Finally, in [20], the SNR p.d.f. computed with HGM was numerically integrated to evaluate performance measures, i.e., the outage probability and ergodic capacity.

Thus, on the one hand, our exact studies for $r = 1$ in [19], [20] are limited by the following:

- Nonfull-Rician (i.e., only Rician–Rayleigh) fading assumption.
- Tedious by-hand derivations of the SNR m.g.f. and p.d.f. differential equations.
- Time-consuming numerical integration of the p.d.f. for performance measure evaluation.
- HGM not tried for large N_R and N_T , e.g., as relevant for large MIMO systems [5], [7].

On the other hand, only approximations exist for full-Rician fading and $r = 1$ [15], [17], [18].

²Other examples: rational functions, logarithm, exponential, sine, special functions (orthogonal polynomials, Bessel [30, p. 41]).

C. Problem Tackled in the Current Work; Exact Analysis and Evaluation Approaches

To the best of our knowledge, the performance of MIMO ZF has not yet been studied *exactly* under full-Rician fading even for $r = 1$. We pursue this study herein, as follows.

First, upon applying a sequence of matrix transformations and results from multivariate statistics, we obtain several theoretical results that help express exactly the SNR m.g.f. as an infinite series with terms in ${}_1F_1(\cdot, \cdot, \cdot)$. Thus, the m.g.f. can be rewritten as a double-infinite series of gamma distribution m.g.f.'s, which readily yields analogous series for the SNR p.d.f. and for the performance measures. Then, they are recast as a generic single-infinite series. However, its truncation is found to incur numerical divergence with increasing K , N_R , and N_T . Consequently, as in [19], it is necessary to derive satisfied differential equations and apply HGM.

Because by-hand derivation of differential equations for our generic series appears intractable, we resort to a novel automated derivation approach using the `HolonomicFunctions` package written earlier by one of the authors [30], [31] and implementing recent advances in computer algebra. It exploits, for holonomic functions, closure properties [20, Section IV.C], [30], the algebraic concept of *Gröbner bases*³, [33], and *creative telescoping* algorithms [30, Ch. 3] to systematically deduce differential equations for their addition, multiplication, composition, and integration. This computer-algebra-aided approach readily yields differential equations not only for the SNR m.g.f. and p.d.f., but also for the outage probability and ergodic capacity.

Finally, we evaluate ZF performance measures by HGM, i.e., by solving the obtained differential equations starting from initial conditions computed with the infinite series.

D. Contributions

Compared to previous MIMO ZF work by us and others, herein we:

- Tackle full-Rician fading with $r = 1$ in a new exact analysis that reveals that the SNR distribution is an infinite mixture of gamma distributions. This SNR distribution yields insight into the effect of channel matrix statistics (mean, correlation) on performance, and helps reassess the approximation with the gamma distribution we studied in [18], [21].

³Buchberger's algorithm [32] for Gröbner basis computation specializes, for example, to the Euclidean algorithm when applied to univariate polynomials, and to Gaussian elimination when applied to linear polynomials in several variables [33]. Gröbner bases have helped solve communications optimization problems cast as systems of polynomial equations, e.g., for interference alignment [34], coding gain maximization in space-time coding [35]; other relevant applications are listed in [33].

- Use computer algebra to automate deductions of differential equations also for performance measures and, thus, also avoid time-consuming numerical integration of the SNR p.d.f..
- Demonstrate that HGM yields accurate performance evaluation for realistic values for K , and even for large N_R and N_T , unlike the infinite series alone and faster than by simulation.
- Exactly average the ZF performance over WINNER II distributions of K and AS.

E. Paper Organization

Section II introduces our model. Section III employs matrix transformations and multivariate statistics to express exactly the m.g.f. of the ZF SNR. Section IV derives a generic infinite series for the SNR m.g.f. and p.d.f., as well as for ZF performance measures. Section V describes the automated derivation of differential equations, which has been accomplished with `HolonomicFunctions` commands as shown in [36]. Finally, Section VI presents numerical results obtained by simulation, series truncation, and HGM. The Appendix shows some proofs and derivation details.

F. Notation

- Scalars, vectors, and matrices are represented with lowercase italics, lowercase boldface, and uppercase boldface, respectively, e.g., y , \mathbf{h} , and \mathbf{H} ; the statement $\mathbf{H} \doteq N_R \times N_T$ indicates N_R rows and N_T columns for \mathbf{H} ; zero vectors and matrices of appropriate dimensions are denoted with $\mathbf{0}$; superscripts \cdot^T and \cdot^H stand for transpose and Hermitian (i.e., complex-conjugate) transpose; \mathbf{I}_N is the $N \times N$ identity matrix.
- $[\cdot]_i$ is the i th element of a vector; $[\cdot]_{i,j}$, $[\cdot]_{i,\bullet}$, and $[\cdot]_{\bullet,j}$ indicate the i, j th element, i th row, and j th column of a matrix; $\|\mathbf{H}\|^2 = \sum_{i=1}^{N_R} \sum_{j=1}^{N_T} |[\mathbf{H}]_{i,j}|^2$ is the squared Frobenius norm.
- $i = 1 : N$ stands for the enumeration $i = 1, 2, \dots, N$; \otimes stands for the Kronecker product [37, p. 72]; \propto stands for ‘proportional to’; \Rightarrow stands for logical implication.
- $\mathbf{h} \sim \mathcal{CN}_{N_R}(\mathbf{h}_d, \mathbf{R})$ denotes an $N_R \times 1$ complex-valued circularly-symmetric Gaussian vector with mean \mathbf{h}_d and covariance matrix \mathbf{R} ; an $N_R \times N_T$ complex-valued circularly-symmetric Gaussian random matrix with mean \mathbf{H}_d , row covariance \mathbf{I}_{N_R} , and column covariance \mathbf{R}_T , i.e., a matrix whose vectorized form is distributed as $\text{vec}(\mathbf{H}^H) \sim \mathcal{CN}_{N_R N_T}(\text{vec}(\mathbf{H}_d^H), \mathbf{I}_{N_R} \otimes \mathbf{R}_T)$, is denoted herein as $\mathbf{H} \sim \mathcal{CN}_{N_R, N_T}(\mathbf{H}_d, \mathbf{I}_{N_R} \otimes \mathbf{R}_T)$, based on the definition from [13]; subscripts \cdot_d and \cdot_r identify, respectively, deterministic and random components; subscript

\cdot_n indicates a normalized variable; $\mathbb{E}\{\cdot\}$ denotes statistical average; $\Gamma(N, \Gamma_1)$ represents the *gamma* distribution with shape parameter N and scale parameter Γ_1 ; $\chi_m^2(\delta)$ denotes the noncentral *chi-square* distribution with m degrees of freedom and noncentrality parameter δ ; χ_m^2 denotes the central chi-square distribution with m degrees of freedom; $B(N, M)$ represents the central *beta* distribution with shape parameters N and M ; $B(N, M, x)$ represents the noncentral beta distribution with shape parameters N and M , and noncentrality x .

- ${}_1F_1(\cdot; \cdot; \cdot)$ is the *confluent hypergeometric function* [38, Eq. (13.2.2)]; $(N)_n$ is the Pochhammer symbol, i.e., $(N)_0 = 1$ and $(N)_n = N(N+1) \dots (N+n-1)$, $\forall n \geq 1$.
- $\partial_t^k g(t, z)$ denotes the k th partial derivative w.r.t. t of function $g(t, z)$.

II. MODEL AND ASSUMPTIONS

A. Received Signal and Fading Models

We consider an uncoded point-to-point uplink MIMO spatial multiplexing system over a frequency-flat fading channel [1, Chs. 3, 7]. There are $N_T \geq 2$ and $N_R \geq N_T$ antenna elements at the transmitter⁴ and receiver, respectively. For the transmit-symbol vector denoted with

$$\mathbf{y} = (y_1 \ y_2 \ \dots \ y_{N_T})^T \doteq N_T \times 1, \quad (1)$$

the stream of complex-valued symbols y_i from antenna i is referred to as Stream i . Without loss of generality, we consider Stream 1 as the intended stream (i.e., whose symbol is detected, and whose detection performance is analyzed and evaluated), and the remaining

$$N_I = N_T - 1 \quad (2)$$

streams, i.e., Streams $i = 2 : N_T$, as interfering streams. The number of *degrees of freedom* is

$$N = N_R - N_I = N_R - N_T + 1. \quad (3)$$

Then, the received signal vector can be represented as

$$\mathbf{r} = \sqrt{\frac{E_s}{N_T}} \mathbf{H} \mathbf{y} + \mathbf{n} \doteq N_R \times 1, \quad (4)$$

⁴For $N_T = 1$ and maximal-ratio combining (MRC), we obtained a simple SNR m.g.f. expression for Rician fading in [19, Eq. (36)].

where $\frac{E_s}{N_T}$ is the energy transmitted per symbol (i.e., per antenna), and $\mathbf{n} \sim \mathcal{CN}_{N_R}(\mathbf{0}, N_0 \mathbf{I}_{N_R})$ is the additive noise. Then, the per-symbol transmit SNR is

$$\Gamma_s = \frac{E_s}{N_0} \frac{1}{N_T}. \quad (5)$$

Finally, we assume that the complex-valued channel matrix $\mathbf{H} \doteq N_R \times N_T$ is Gaussian (more details follow below), has rank N_T , and is perfectly known at the receiver⁵. With its deterministic and random components denoted as \mathbf{H}_d and \mathbf{H}_r , respectively, we can write

$$\mathbf{H} = \mathbf{H}_d + \mathbf{H}_r = \sqrt{\frac{K}{K+1}} \mathbf{H}_{d,n} + \sqrt{\frac{1}{K+1}} \mathbf{H}_{r,n}, \quad (6)$$

where $\mathbf{H}_{d,n}$ and $\mathbf{H}_{r,n}$ are the components of \mathbf{H} normalized as

$$\|\mathbf{H}_{d,n}\|^2 = \mathbb{E}\{\|\mathbf{H}_{r,n}\|^2\} = N_R N_T, \text{ i.e., } \mathbb{E}\{\|\mathbf{H}\|^2\} = N_R N_T, \quad (7)$$

and K , known as the Rician K -factor, is described by

$$K = \frac{\|\mathbf{H}_d\|^2}{\mathbb{E}\{\|\mathbf{H}_r\|^2\}} = \frac{\frac{K}{K+1} \|\mathbf{H}_{d,n}\|^2}{\frac{1}{K+1} \mathbb{E}\{\|\mathbf{H}_{r,n}\|^2\}}. \quad (8)$$

Then, $K = 0$ yields full-Rayleigh fading, i.e., $|\mathbf{H}_{i,j}|$ is Rayleigh distributed $\forall i, j$, as assumed in [8], [9], [10]. Further, the case when $K \neq 0$ and in $\mathbf{H}_{d,n}$ only column $[\mathbf{H}_{d,n}]_{\bullet,1}$ is nonzero is referred to as Rician-Rayleigh fading, as in [19], [20]. Finally, herein, the case when $K \neq 0$ and each column of $\mathbf{H}_{d,n}$ has at least one nonzero element is referred to as full-Rician fading.

We assume that \mathbf{H}_d arises due to LoS propagation between transmitter and receiver. Then, if the transmitter-receiver distance is much larger than the antenna interelement spacing, \mathbf{H}_d can be represented as the outer product of the array response vectors for the receiving antenna, $\mathbf{a} \doteq N_R \times 1$, and transmitting antenna, $\mathbf{b} \doteq N_T \times 1$, i.e., [1, Eq. (7.29), p. 299]

$$\mathbf{H}_d = \mathbf{a} \mathbf{b}^H = \mathbf{a} (b_1^* \ b_2^* \ \dots \ b_{N_T}^*), \quad (9)$$

which reveals that \mathbf{H}_d has rank $r = 1$ and columns given by $\mathbf{h}_{d,i} = \mathbf{a} b_i^*, i = 1 : N_T$.

Remark 1. We may assume that $\|\mathbf{a}\| = 1$ if we scale \mathbf{b} according to

$$\|\mathbf{b}\|^2 = \sum_{i=1}^{N_T} |b_i|^2 = \sum_{i=1}^{N_T} \underbrace{\|\mathbf{a}\|^2}_{=1} |b_i|^2 = \sum_{i=1}^{N_T} \|\mathbf{h}_{d,i}\|^2$$

⁵ZF for imperfectly-known \mathbf{H} can be studied, e.g., with the effective-SNR approach we described in [18].

$$= \|\mathbf{H}_d\|^{2^{(6),(7)}} \frac{K}{K+1} N_R N_T. \quad (10)$$

For a tractable analysis, we assume zero row correlation (i.e., receive-antenna correlation) for \mathbf{H} . On the other hand, we assume, as in [9], [10], [19], [20], that any row of $\mathbf{H}_{r,n}$ has the same distribution $\mathcal{CN}_{N_T}(\mathbf{0}, \mathbf{R}_T)$, so that any row of \mathbf{H}_r has the same distribution $\mathcal{CN}_{N_T}(\mathbf{0}, \mathbf{R}_{T,K})$ with

$$\begin{aligned} \mathbf{R}_{T,K} &= \frac{1}{N_R} \mathbb{E}\{\mathbf{H}_r^H \mathbf{H}_r\} = \frac{1}{K+1} \frac{1}{N_R} \mathbb{E}\{\mathbf{H}_{r,n}^H \mathbf{H}_{r,n}\} \\ &= \frac{1}{K+1} \mathbf{R}_T. \end{aligned} \quad (11)$$

Thus, we can write $\mathbf{H}_r = \mathbf{H}_w \mathbf{R}_{T,K}^{1/2}$ with $\mathbf{H}_w \sim \mathcal{CN}_{N_R, N_T}(\mathbf{0}, \mathbf{I}_{N_R} \otimes \mathbf{I}_{N_T})$, so that $\mathbf{H} = \mathbf{H}_d + \mathbf{H}_r \sim \mathcal{CN}_{N_R, N_T}(\mathbf{H}_d, \mathbf{I}_{N_R} \otimes \mathbf{R}_{T,K})$.

Matrix \mathbf{R}_T is determined by antenna interelement spacing and AS, i.e., the ‘standard deviation’ of the power azimuth spectrum [23, p. 136]. When the latter is modeled as Laplacian, as recommended by WINNER II [22], \mathbf{R}_T can be computed from the AS with [23, Eqs. (4-3)–(4-5)].

Remark 2. *WINNER II modeled the measured AS (in degrees) and K (in dB) as random variables with scenario-dependent lognormal distributions [22, Table 5.5] [18, Table 1]. Thus, herein, we attempt to evaluate ZF performance for AS and K values relevant to these distributions.*

B. Matrix Partitioning Used in Analysis

To study Stream-1 detection performance, we shall employ the partitioning

$$\mathbf{H} = (\mathbf{h}_1 \quad \mathbf{H}_2) = (\mathbf{h}_{d,1} \quad \mathbf{H}_{d,2}) + (\mathbf{h}_{r,1} \quad \mathbf{H}_{r,2}), \quad (12)$$

where \mathbf{h}_1 , $\mathbf{h}_{d,1}$, and $\mathbf{h}_{r,1}$ are $N_R \times 1$ vectors, whereas \mathbf{H}_2 , $\mathbf{H}_{d,2}$, and $\mathbf{H}_{r,2}$ are $N_R \times N_I$ matrices.

We shall also employ the corresponding partitioning of the column covariance matrix:

$$\mathbf{R}_{T,K} = \begin{pmatrix} \mathbf{R}_{T,K_{11}} & \mathbf{R}_{T,K_{12}} \\ \mathbf{R}_{T,K_{21}} & \mathbf{R}_{T,K_{22}} \end{pmatrix} = \begin{pmatrix} r_{T,K_{11}} & \mathbf{r}_{T,K_{21}}^H \\ \mathbf{r}_{T,K_{21}} & \mathbf{R}_{T,K_{22}} \end{pmatrix}. \quad (13)$$

Remark 3. *Herein, we consider full-Rician fading with $r = \text{rank}(\mathbf{H}_d) = \text{rank}(\mathbf{H}_{d,2}) = 1$, whereas in [19], [20] we considered its special case of Rician-Rayleigh fading, i.e., $\text{rank}(\mathbf{H}_d) = 1$, but $\text{rank}(\mathbf{H}_{d,2}) = 0$. Thus, the results obtained herein specialize to those in [19], [20] when we reduce to $\mathbf{0}$ the vector formed with the last $N_I = N_T - 1$ elements of \mathbf{b} , i.e., the vector*

$$\tilde{\mathbf{b}} = (b_2 \quad \dots \quad b_{N_T})^T. \quad (14)$$

III. EXACT ANALYSIS OF ZF SNR

A. ZF SNR as Hermitian Form

Given \mathbf{H} , ZF for the signal from (4) refers to symbol detection based on the operation

$$\sqrt{\frac{N_T}{E_s}} [\mathbf{H}^H \mathbf{H}]^{-1} \mathbf{H}^H \mathbf{r} = \mathbf{y} + \frac{1}{\sqrt{\Gamma_s}} [\mathbf{H}^H \mathbf{H}]^{-1} \mathbf{H}^H \frac{\mathbf{n}}{\sqrt{N_0}}. \quad (15)$$

Based on (15) and [10], [19], the SNR for Stream 1 can be written as the Hermitian form below:

$$\gamma_1 = \frac{\Gamma_s}{[(\mathbf{H}^H \mathbf{H})^{-1}]_{1,1}} = \Gamma_s \mathbf{h}_1^H \underbrace{[\mathbf{I}_{N_R} - \mathbf{H}_2 (\mathbf{H}_2^H \mathbf{H}_2)^{-1} \mathbf{H}_2^H]}_{=\mathbf{Q}_2} \mathbf{h}_1, \quad (16)$$

where $\mathbf{Q}_2 \doteq N_R \times N_R$ is idempotent and of rank N .

Remark 4. The following transformations do not change the ZF SNR in (16):

- Row transformations of \mathbf{H} with unitary matrices, because they do not change $\mathbf{H}^H \mathbf{H}$.
- Column transformations of \mathbf{H}_2 with nonsingular matrices, because they do not change \mathbf{Q}_2 .

Several such transformations, shown below, help derive the exact SNR distribution.

B. Row Transformation $\mathbf{F} = \mathbf{V}\mathbf{H}$ That Zeroes Rows $[\mathbf{F}_d]_{i,\bullet}$, $i = 2 : N_R$

If we make the substitution $\mathbf{H} = \mathbf{V}^H \mathbf{F}$, with unitary $\mathbf{V} \doteq N_R \times N_R$, in (16) and partition according to (12) the matrix

$$\begin{aligned} \mathbf{F} &= \mathbf{V}\mathbf{H} \doteq N_R \times N_T \\ &= (\mathbf{f}_1 \quad \mathbf{F}_2) = (\mathbf{f}_{d,1} \quad \mathbf{F}_{d,2}) + (\mathbf{f}_{r,1} \quad \mathbf{F}_{r,2}), \end{aligned} \quad (17)$$

the ZF SNR Hermitian form in (16) becomes

$$\gamma_1 = \Gamma_s \mathbf{f}_1^H \mathbf{Q}_2 \mathbf{f}_1, \quad (18)$$

with

$$\mathbf{Q}_2 = \mathbf{I}_{N_R} - \mathbf{F}_2 (\mathbf{F}_2^H \mathbf{F}_2)^{-1} \mathbf{F}_2^H. \quad (19)$$

Choosing the first row of the unitary matrix \mathbf{V} as $[\mathbf{V}]_{1,\bullet} = \mathbf{a}^H$, we conveniently obtain

$$\begin{aligned} [\mathbf{F}_d]_{1,\bullet} &\stackrel{(9)}{=} ([\mathbf{V}]_{1,\bullet} \mathbf{a}) \mathbf{b}^H = \|\mathbf{a}\|^2 \mathbf{b}^H = \mathbf{b}^H, \\ [\mathbf{F}_d]_{i,\bullet} &\stackrel{(9)}{=} \underbrace{([\mathbf{V}]_{i,\bullet} \mathbf{a})}_{=0} \mathbf{b}^H = \mathbf{0}, \quad i = 2 : N_R, \end{aligned}$$

$$\text{i.e., } [\mathbf{F}_d]_{\bullet,j} = \mathbf{f}_{d,j} = (b_j^* \ 0 \ \dots \ 0)^\top, j = 1 : N_T. \quad (20)$$

Theorem 1. *The m.g.f. of the SNR conditioned on \mathbf{Q}_2 can be written, simply, as*

$$\begin{aligned} M_{\gamma_1|\mathbf{Q}_2}(s) &= \mathbb{E}_{\gamma_1}\{e^{s\gamma_1}|\mathbf{Q}_2\} \\ &= \frac{1}{(1 - \Gamma_1 s)^N} \exp\{f_1(s)[\mathbf{Q}_2]_{1,1}\}, \end{aligned} \quad (21)$$

with scalar Γ_1 and function $f_1(s)$ defined in the proof below.

Proof: Because the column covariance of $\mathbf{F} = \mathbf{V}\mathbf{H}$ is the same as that of \mathbf{H} , i.e., $\mathbf{R}_{T,K}$, partitioned as in (13), and because $\mathbf{f}_1 \doteq N_R \times 1$ and $\mathbf{F}_2 \doteq N_R \times N_I$ from the partitioning of \mathbf{F} in (17) are jointly Gaussian, the distribution of \mathbf{f}_1 given \mathbf{F}_2 is given by [10, Appendix], [19, Eqs. (12)–(16)]

$$\begin{aligned} \mathbf{f}_1|\mathbf{F}_2 &\sim \mathcal{CN}_{N_R}\left(\underbrace{(\mathbf{f}_{d,1} - \mathbf{F}_{d,2}\mathbf{r}_{2,1})}_{=\boldsymbol{\mu} \doteq N_R \times 1} + \mathbf{F}_2\mathbf{r}_{2,1}, \right. \\ &\quad \left. \left([\mathbf{R}_{T,K}^{-1}]_{1,1}\right)^{-1} \mathbf{I}_{N_R}\right), \end{aligned} \quad (22)$$

with

$$\mathbf{r}_{2,1} = \mathbf{R}_{T,K_{22}}^{-1} \mathbf{r}_{T,K_{21}} \doteq N_I \times 1, \quad (23)$$

$$\left([\mathbf{R}_{T,K}^{-1}]_{1,1}\right)^{-1} = r_{T,K_{11}} - \mathbf{r}_{T,K_{21}}^H \mathbf{R}_{T,K_{22}}^{-1} \mathbf{r}_{T,K_{21}}. \quad (24)$$

Then, it can be shown by substituting (22) into (18) and further manipulating as in [10], [19], that the SNR conditioned on \mathbf{Q}_2 from (18) can be written as the Hermitian form

$$\gamma_1|\mathbf{Q}_2 = \Gamma_1 \tilde{\mathbf{f}}_1^H \mathbf{Q}_2 \tilde{\mathbf{f}}_1, \quad \text{with} \quad (25)$$

$$\Gamma_1 = \frac{\Gamma_s}{[\mathbf{R}_{T,K}^{-1}]_{1,1}}, \quad (26)$$

$$\tilde{\mathbf{f}}_1 \sim \mathcal{CN}_{N_R}\left(\sqrt{[\mathbf{R}_{T,K}^{-1}]_{1,1}} \boldsymbol{\mu}, \mathbf{I}_{N_R}\right), \quad (27)$$

$$\begin{aligned} \boldsymbol{\mu} &\stackrel{(22)}{=} \mathbf{f}_{d,1} - \mathbf{F}_{d,2}\mathbf{r}_{2,1} \stackrel{(20)}{=} (b_1^* - \tilde{\mathbf{b}}^H \mathbf{r}_{2,1} \ 0 \ \dots \ 0)^\top \\ &= (\mu_1 \ 0 \ \dots \ 0)^\top, \end{aligned} \quad (28)$$

i.e., row transformation $\mathbf{F} = \mathbf{V}\mathbf{H}$ yielded a single nonzero-mean element in $\tilde{\mathbf{f}}_1$, which simplifies the ensuing analysis.

The Hermitian form in $\tilde{\mathbf{f}}_1$ from (25) helps cast the m.g.f. of the SNR given \mathbf{Q}_2 as [19, Eq. (20)]

$$M_{\gamma_1|\mathbf{Q}_2}(s) = \frac{\exp \left\{ -x_1 \boldsymbol{\nu}^H [\mathbf{I}_{N_R} - (\mathbf{I}_{N_R} - \Gamma_1 s \mathbf{Q}_2)^{-1}] \boldsymbol{\nu} \right\}}{\det (\mathbf{I}_{N_R} - \Gamma_1 s \mathbf{Q}_2)}, \quad (29)$$

with

$$x_1 = [\mathbf{R}_{T,K}^{-1}]_{1,1} \|\boldsymbol{\mu}\|^2 = [\mathbf{R}_{T,K}^{-1}]_{1,1} |\mu_1|^2, \quad (30)$$

$$\boldsymbol{\nu} = \frac{\boldsymbol{\mu}}{\mu_1} = (1 \ 0 \ \dots \ 0)^T, \quad (31)$$

$$\mathbf{I}_{N_R} - (\mathbf{I}_{N_R} - \Gamma_1 s \mathbf{Q}_2)^{-1} = -\frac{\Gamma_1 s}{1 - \Gamma_1 s} \mathbf{Q}_2. \quad (32)$$

Above, (32) follows by using the eigendecomposition of \mathbf{Q}_2 . The desired m.g.f. expression in (21) follows by substituting (32) into (29) and defining $f_1(s) = \frac{\Gamma_1 s}{1 - \Gamma_1 s} x_1$. ■

C. Partial Column Transformations That Help Rewrite $[\mathbf{Q}_2]_{1,1}$ Conveniently

1) *Unitary Transformation $\mathbf{E}_2 = \mathbf{F}_2 \tilde{\mathbf{V}}$ That Zeroes Elements $[\mathbf{E}_{d,2}]_{1,j}$, $j = 2 : N_I$:* Making the substitution $\mathbf{F}_2 = \mathbf{E}_2 \tilde{\mathbf{V}}^H$, with unitary $\tilde{\mathbf{V}} \doteq N_I \times N_I$, in (19) yields

$$\mathbf{Q}_2 = \mathbf{I}_{N_R} - \mathbf{E}_2 (\mathbf{E}_2^H \mathbf{E}_2)^{-1} \mathbf{E}_2^H. \quad (33)$$

Based on (17), we can write

$$\mathbf{E}_2 = \mathbf{F}_2 \tilde{\mathbf{V}} = \mathbf{F}_{d,2} \tilde{\mathbf{V}} + \mathbf{F}_{r,2} \tilde{\mathbf{V}} = \mathbf{E}_{d,2} + \mathbf{E}_{r,2} \doteq N_R \times N_I. \quad (34)$$

Setting $[\tilde{\mathbf{V}}]_{\bullet,1} = \tilde{\mathbf{b}}/\|\tilde{\mathbf{b}}\|$ simplifies the ensuing SNR analysis as it zeroes $[\mathbf{E}_{d,2}]_{1,j}$, $j = 2 : N_I$:

$$\begin{aligned} \mathbf{E}_{d,2} &= \mathbf{F}_{d,2} \tilde{\mathbf{V}} \stackrel{(20)}{=} \begin{pmatrix} \tilde{\mathbf{b}}^H \\ \mathbf{0} \end{pmatrix} \begin{pmatrix} \frac{\tilde{\mathbf{b}}}{\|\tilde{\mathbf{b}}\|} & [\tilde{\mathbf{V}}]_{\bullet,2} \cdots [\tilde{\mathbf{V}}]_{\bullet,N_I} \end{pmatrix} \\ &= \|\tilde{\mathbf{b}}\| \begin{pmatrix} 1 & \mathbf{0} \\ \mathbf{0} & \mathbf{0} \end{pmatrix}. \end{aligned} \quad (35)$$

2) *Nonsingular Transformation That Decorrelates the Columns of \mathbf{E}_2 :* For the column correlation of $\mathbf{E}_{r,2}$ from (34), i.e., for

$$\begin{aligned} \frac{1}{N_R} \mathbb{E}\{\mathbf{E}_{r,2}^H \mathbf{E}_{r,2}\} &= \frac{1}{N_R} \mathbb{E}\{(\mathbf{F}_{r,2} \tilde{\mathbf{V}})^H (\mathbf{F}_{r,2} \tilde{\mathbf{V}})\} \\ &\stackrel{(13)}{=} \tilde{\mathbf{V}}^H \mathbf{R}_{T,K_{22}} \tilde{\mathbf{V}}, \end{aligned} \quad (36)$$

let us consider the Cholesky decomposition [37, Sec. 5.6]

$$\tilde{\mathbf{V}}^H \mathbf{R}_{T,K_{22}} \tilde{\mathbf{V}} = \mathbf{A} \mathbf{A}^H, \quad (37)$$

where $\mathbf{A} \doteq N_I \times N_I$ is upper triangular with real-valued and positive diagonal elements.

Then, considering matrix $\mathbf{E}_{w,2} \sim \mathcal{CN}_{N_R, N_I}(\mathbf{0}, \mathbf{I}_{N_R} \otimes \mathbf{I}_{N_I})$, we can write (34) based on (37) and (36) as

$$\mathbf{E}_2 = \mathbf{E}_{d,2} + \mathbf{E}_{w,2} \mathbf{A}^H = (\mathbf{E}_{d,2} \mathbf{A}^{-H} + \mathbf{E}_{w,2}) \mathbf{A}^H. \quad (38)$$

Thus, by transforming the columns of \mathbf{E}_2 with \mathbf{A}^{-H} , we obtain

$$\mathbf{G}_2 = \mathbf{E}_2 \mathbf{A}^{-H} = \mathbf{E}_{d,2} \mathbf{A}^{-H} + \mathbf{E}_{w,2} \doteq N_R \times N_I, \quad (39)$$

whose mean that can be written, based on (35) and the fact that \mathbf{A}^{-H} is lower triangular, as

$$\mathbf{G}_{d,2} = \mathbf{E}_{d,2} \mathbf{A}^{-H} = \|\tilde{\mathbf{b}}\| [\mathbf{A}^{-H}]_{1,1} \begin{pmatrix} 1 & \mathbf{0} \\ \mathbf{0} & \mathbf{0} \end{pmatrix}. \quad (40)$$

Using (37), the properties of \mathbf{A} , and the choice $[\tilde{\mathbf{V}}]_{\bullet,1} = \tilde{\mathbf{b}}/\|\tilde{\mathbf{b}}\|$, the squared norm of $\mathbf{G}_{d,2}$ can be written as

$$x_2 = \|\mathbf{G}_{d,2}\|^2 = \tilde{\mathbf{b}}^H \mathbf{R}_{T,K_{22}}^{-1} \tilde{\mathbf{b}}. \quad (41)$$

Remark 5. For Rician-Rayleigh fading, Remark 3 revealed that $\tilde{\mathbf{b}} = \mathbf{0}$, which by (41) implies $x_2 = 0$. On the other hand, for full-Rayleigh fading, (30) implies that also $x_1 = 0$.

Thus, column transformation (39) yielded \mathbf{G}_2 with uncorrelated columns and mean given by

$$[\mathbf{G}_{d,2}]_{i,j} = \begin{cases} \sqrt{x_2} & , (\text{i.e., real-valued}) \text{ for } i = j = 1, \\ 0 & , \text{otherwise.} \end{cases} \quad (42)$$

Substituting $\mathbf{E}_2 = \mathbf{G}_2 \mathbf{A}^H$ into (33) yields

$$\mathbf{Q}_2 = \mathbf{I}_{N_R} - \mathbf{G}_2 (\mathbf{G}_2^H \mathbf{G}_2)^{-1} \mathbf{G}_2^H. \quad (43)$$

The simple statistics of \mathbf{G}_2 (vs. \mathbf{F}_2) help simplify our SNR distribution analysis, as shown below.

3) *QR Decomposition:* Finally, by substituting in (43) the QR decomposition [37, Sec. 5.7]

$$\mathbf{G}_2 = \mathbf{U}_2 \mathbf{T}_2, \quad (44)$$

where $\mathbf{U}_2 \doteq N_R \times N_I$ satisfies $\mathbf{U}_2^H \mathbf{U}_2 = \mathbf{I}_{N_I}$, and $\mathbf{T}_2 \doteq N_I \times N_I$ is upper triangular with real-valued and positive diagonal elements, we can write \mathbf{Q}_2 simply as

$$\mathbf{Q}_2 = \mathbf{I}_{N_R} - \mathbf{U}_2 \mathbf{T}_2 (\mathbf{T}_2^H \mathbf{T}_2)^{-1} \mathbf{T}_2^H \mathbf{U}_2^H = \mathbf{I}_{N_R} - \mathbf{U}_2 \mathbf{U}_2^H. \quad (45)$$

This helps write $[\mathbf{Q}_2]_{1,1}$ for the m.g.f. in (21) solely in terms of the first row of \mathbf{U}_2 as

$$\begin{aligned}
[\mathbf{Q}_2]_{1,1} &= 1 - [\mathbf{U}_2]_{1,\bullet} ([\mathbf{U}_2]_{1,\bullet})^H \\
&= 1 - (|[\mathbf{U}_2]_{1,1}|^2 + |[\mathbf{U}_2]_{1,2}|^2 + \cdots + |[\mathbf{U}_2]_{1,N_I}|^2) \\
&= \underbrace{(1 - |[\mathbf{U}_2]_{1,1}|^2)}_{=\beta_1} \\
&\quad \times \underbrace{\left(1 - \frac{|[\mathbf{U}_2]_{1,2}|^2 + \cdots + |[\mathbf{U}_2]_{1,N_I}|^2}{1 - |[\mathbf{U}_2]_{1,1}|^2}\right)}_{=\beta_2}.
\end{aligned} \tag{46}$$

D. Principal Analysis Result: Exact M.G.F. Expression of the Unconditioned SNR

The above transformations have helped write the conditioned-SNR m.g.f. from (21) as

$$M_{\gamma_1}(s \mid \beta_1, \beta_2) = \frac{1}{(1 - \Gamma_1 s)^N} \exp\{f_1(s)\beta_1\beta_2\}. \tag{47}$$

In order to express the unconditioned-SNR m.g.f., we need to average (47) over the distributions of β_1 and β_2 , which are elucidated in the following two lemmas.

Lemma 1. *Random variable β_1 from (46) is distributed as*

$$\beta_1 \sim \text{B}(N_R - 1, 1, x_2). \tag{48}$$

Proof: See Appendix A. ■

Lemma 2. *Random variable β_2 from (46) is distributed as*

$$\beta_2 \sim \text{B}(N, N_I - 1), \tag{49}$$

i.e., has m.g.f. [19, Eq. (30)]

$$M_{\beta_2}(s) = {}_1F_1(N; N_R - 1; s), \tag{50}$$

and is independent of β_1 .

Proof: See Appendix B. ■

Theorem 2. *The m.g.f. of the unconditioned ZF SNR under full-Rician fading with $r = 1$ is⁶*

$$M_{\gamma_1}(s; x_1, x_2) = \frac{1}{(1 - \Gamma_1 s)^N} \sum_{n_2=0}^{\infty} \frac{e^{-x_2} x_2^{n_2}}{n_2!}$$

⁶We remind that the definitions of scalars Γ_1 , x_1 , and x_2 appear in (26), (30), and (41), respectively.

$$\times {}_1F_1\left(N; n_2 + N_R; \frac{\Gamma_1 s}{1 - \Gamma_1 s} x_1\right). \quad (51)$$

Proof: Due to limited space, we only outline the proof: it follows by successively averaging the m.g.f. of the conditioned SNR in (47) over the distributions of the independent random variables β_1 and β_2 , and by exploiting (50), (53), and (83). ■

E. Effects of Channel Matrix Statistics

For Rician-Rayleigh fading (i.e., for $x_2 = 0$), the SNR m.g.f. from (51) reduces to [19, Eq. (31)]

$$M_{\gamma_1}(s; x_1) = \frac{1}{(1 - \Gamma_1 s)^N} {}_1F_1\left(N; N_R; \frac{\Gamma_1 s}{1 - \Gamma_1 s} x_1\right). \quad (52)$$

Then, for γ_1 , the first two moments, variance $\mathbb{V}\{\gamma_1\} = \mathbb{E}\{\gamma_1^2\} - (\mathbb{E}\{\gamma_1\})^2$, and amount of fading $\mathbb{A}\{\gamma_1\} = \mathbb{V}\{\gamma_1\} / (\mathbb{E}\{\gamma_1\})^2$, i.e., SNR statistics, have been expressed in [19, Table I]. Because the SNR m.g.f. for full-Rician fading from (51) is a weighted infinite series of SNR m.g.f.'s for Rician-Rayleigh fading from (52) with N_R replaced with $N_R + n_2$, writing the SNR statistics for the former from those for the latter from [19, Table I] is trivial.

The effect of x_2 on SNR statistics is not readily discernible from (51) and [19, Table I]. On the other hand, [19, Table I] reveals that $\mathbb{E}\{\gamma_1\}$ increases with N from (3), Γ_1 from (26), and x_1 from (30), whereas $\mathbb{A}\{\gamma_1\}$ decreases with N and x_1 . It can be shown that x_1 is proportional to $\|\mathbf{h}_{d,1} - \mathbf{H}_{d,2}\mathbf{r}_{2,1}\|$. Thus, the performance of ZF for full-Rician fading with $r = 1$ is worst when the channel matrix statistics satisfy condition $\mathbf{h}_{d,1} = \mathbf{H}_{d,2}\mathbf{r}_{2,1}$, and it improves with increasing $\|\mathbf{h}_{d,1} - \mathbf{H}_{d,2}\mathbf{r}_{2,1}\|$. In [21], where we studied full-Rician fading irrespective of r , we had noticed (e.g., by comparing [21, Figs. 1, 2]) that ZF performed worst for $\mathbf{h}_{d,1} = \mathbf{H}_{d,2}\mathbf{r}_{2,1}$.

Remark 6. Note that $\forall x_2$, if $\mathbf{h}_{d,1} = \mathbf{H}_{d,2}\mathbf{r}_{2,1}$, i.e., $x_1 = 0$, then the m.g.f. in (51) reduces to the gamma m.g.f. $M_{\gamma_1}(s) = (1 - \Gamma_1 s)^{-N}$. On the other hand, the gamma distribution with m.g.f. $M(s) = (1 - s\hat{\Gamma}_1)^{-N}$ and $\hat{\Gamma}_1$ obtained as in (26) from $\hat{\mathbf{R}}_{T,K} = \mathbf{R}_{T,K} + \frac{1}{N_R}\mathbf{H}_d^H\mathbf{H}_d$, has previously been employed to approximate the actual ZF SNR distribution for Rician fading, irrespective of r — see [18], [29] and references therein. Interestingly, condition $\mathbf{h}_{d,1} = \mathbf{H}_{d,2}\mathbf{r}_{2,1}$ yields $\Gamma_1 = \hat{\Gamma}_1$, rendering the approximation exact — see [21, Corollary 4].

The above have yielded the following insights.

Remark 7. For ZF under full-Rician fading with $r = 1$, condition $\mathbf{h}_{d,1} = \mathbf{H}_{d,2}\mathbf{r}_{2,1}$ yields: 1) worst performance; 2) full accuracy for the gamma distribution previously employed to approximate the SNR distribution.

IV. EXACT INFINITE SERIES EXPRESSIONS FOR ZF PERFORMANCE MEASURES

A. Infinite Series Expansion of ${}_1F_1(\cdot; \cdot; \sigma)$ Around $\sigma_0 = 0$

Using the well-known infinite series expansion around $\sigma_0 = 0$ [19, Eq. (30)]

$${}_1F_1(N; N_R; \sigma) = \sum_{n=0}^{\infty} \frac{(N)_n}{(N_R)_n} \frac{\sigma^n}{n!}, \quad (53)$$

the SNR m.g.f. from (52) for Rician-Rayleigh fading can also be written as [19, Eq. (37)]

$$\begin{aligned} M_{\gamma_1}(s; x_1) &= \sum_{n_1=0}^{\infty} \frac{(N)_{n_1}}{(N_R)_{n_1}} \frac{x_1^{n_1}}{n_1!} \\ &\times \sum_{m_1=0}^{n_1} \binom{n_1}{m_1} (-1)^{m_1} \underbrace{\frac{1}{(1 - s\Gamma_1)^{N+n_1-m_1}}}_{=M_{n_1, m_1}(s)}, \end{aligned} \quad (54)$$

where $M_{n_1, m_1}(s)$ is the m.g.f. of a random variable distributed as $\Gamma(N + n_1 - m, \Gamma_1)$.

Theoretically, (53) converges $\forall \sigma$. Nevertheless, the computation of (53) by truncation incurs inherent numerical convergence difficulties with increasing σ [19]. Consequently, the computation of ensuing measures, e.g., the ZF SNR p.d.f., becomes nontrivial at realistic values of K , as revealed in [19], [20]. Similar difficulties arise also for the case studied herein, i.e., full-Rician fading with $r = 1$, upon infinite series expansion of ${}_1F_1(\cdot; \cdot; \sigma)$ in the SNR m.g.f. expression from (51), as discussed below.

B. Exact Double-Infinite Series for M.G.F., P.D.F., and Performance Measures

By substituting (53) into (51) and proceeding as for (54), the SNR m.g.f. becomes

$$\begin{aligned} M_{\gamma_1}(s; x_1, x_2) &= e^{-x_2} \sum_{n_1=0}^{\infty} \sum_{n_2=0}^{\infty} \frac{(N)_{n_1}}{(n_2 + N_R)_{n_1}} \frac{x_1^{n_1}}{n_1!} \frac{x_2^{n_2}}{n_2!} \\ &\times \underbrace{\sum_{m_1=0}^{n_1} \binom{n_1}{m_1} (-1)^{m_1} M_{n_1, m_1}(s)}_{=M_{n_1}(s)}. \end{aligned} \quad (55)$$

Using the m.g.f.–p.d.f. Laplace-transform pair corresponding to $\Gamma(N + n_1 - m, \Gamma_1)$, i.e.,

$$M_{n_1, m_1}(s) = \frac{1}{(1 - s\Gamma_1)^{N+n_1-m_1}}, \quad (56)$$

$$p_{n_1, m_1}(t) = \frac{t^{(N+n_1-m_1)-1} e^{-t/\Gamma_1}}{[(N + n_1 - m_1) - 1]! \Gamma_1^{N+n_1-m_1}}, \quad (57)$$

the ZF SNR p.d.f. corresponding to (55) can be written, analogously, as⁷:

$$\begin{aligned} p_{\gamma_1}(t; x_1, x_2) &= e^{-x_2} \sum_{n_1=0}^{\infty} \sum_{n_2=0}^{\infty} \frac{(N)_{n_1}}{(n_2 + N_R)_{n_1}} \frac{x_1^{n_1}}{n_1!} \frac{x_2^{n_2}}{n_2!} \\ &\quad \times \underbrace{\sum_{m_1=0}^{n_1} \binom{n_1}{m_1} (-1)^{m_1} p_{n_1, m_1}(t)}_{=p_{n_1}(t)}. \end{aligned} \quad (58)$$

By integrating (58), the Stream-1 outage probability at threshold SNR τ and the ergodic capacity (i.e., rate) are exactly characterized by analogous infinite series, i.e.,

$$P_o(x_1, x_2) = \int_0^{\tau} p_{\gamma_1}(t; x_1, x_2) dt \quad (59)$$

$$\begin{aligned} &= e^{-x_2} \sum_{n_1=0}^{\infty} \sum_{n_2=0}^{\infty} \frac{(N)_{n_1}}{(n_2 + N_R)_{n_1}} \frac{x_1^{n_1}}{n_1!} \frac{x_2^{n_2}}{n_2!} \\ &\quad \times \underbrace{\sum_{m_1=0}^{n_1} \binom{n_1}{m_1} (-1)^{m_1} P_{o, n_1, m_1}}_{=P_{o, n_1}}, \end{aligned} \quad (60)$$

$$C(x_1, x_2) = \frac{1}{\ln 2} \int_0^{\infty} \ln(1+t) p_{\gamma_1}(t; x_1, x_2) dt \quad (61)$$

$$\begin{aligned} &= e^{-x_2} \sum_{n_1=0}^{\infty} \sum_{n_2=0}^{\infty} \frac{(N)_{n_1}}{(n_2 + N_R)_{n_1}} \frac{x_1^{n_1}}{n_1!} \frac{x_2^{n_2}}{n_2!} \\ &\quad \times \underbrace{\sum_{m_1=0}^{n_1} \binom{n_1}{m_1} (-1)^{m_1} C_{n_1, m_1}}_{=C_{n_1}}, \end{aligned} \quad (62)$$

where⁸

$$P_{o, n_1, m_1} = \int_0^{\tau} p_{n_1, m_1}(t) dt = \frac{\gamma(N + n_1 - m_1, \tau/\Gamma_1)}{[(N + n_1 - m_1) - 1]!}, \quad (63)$$

⁷An alternate p.d.f. expression, for real-valued \mathbf{H} , appears in [39, Eq. (31)].

⁸ $\gamma(k, x) = \int_0^x t^{k-1} e^{-t} dt$ is the *incomplete gamma function* [38, p. 174]. Integral (64) is expressed in [19, Eq. (73)].

$$C_{n_1, m_1} = \frac{1}{\ln 2} \int_0^\infty \ln(1+t) p_{n_1, m_1}(t) dt. \quad (64)$$

Finally, the approach in [19, Section V.A] can help express also the average error probability as an infinite series analogous to (60) and (62).

On the other hand, the previously employed approximating gamma distribution for the ZF SNR mentioned in Remark 6 yields simple performance measures expressions similar to (63) and (64).

C. Generic Single-Infinite Series for M.G.F., P.D.F., and Performance Measures

Because (55), (58), (60), and (62) are analogous, we may represent them as the generic double infinite series

$$h(x_1, x_2) = e^{-x_2} \sum_{n_1=0}^{\infty} \sum_{n_2=0}^{\infty} \frac{(N)_{n_1}}{(N_R + n_2)_{n_1}} H_{n_1} \frac{x_1^{n_1}}{n_1!} \frac{x_2^{n_2}}{n_2!}, \quad (65)$$

where H_{n_1} stands for $M_{n_1}(s)$ from (55), $p_{n_1}(t)$ from (58), P_{o, n_1} from (60), and C_{n_1} from (62). Thus, the dependence of $h(x_1, x_2)$ on s for the m.g.f. or t for the p.d.f. is not explicitly shown in (65), for simplicity.

Numerical results not shown due to length limitations have revealed that increasing K , N_R , and N_T yield increasingly problematic numerical convergence for series (65). This is explained by: 1) the fact that (55) has been obtained from (51) by replacing ${}_1F_1\left(N; n_2 + N_R; \frac{\Gamma_1 s}{1 - \Gamma_1 s} x_1\right)$ with its expansion around $x_1 = 0$ from (53); 2) the fact that x_1 is increasing because of the following proportionality, proved in Appendix C:

$$x_1 \propto K N_R N_T. \quad (66)$$

Appendix C also shows that $x_2 \propto K N_R N_T$. Then, the expressions for x_1 and x_2 deduced there in (95) and (96) can be used to show that their ratio $c_1 = \frac{x_1}{x_2}$ is real-valued, positive, and independent of K and N_R . Finally, unshown numerical results have revealed that $c_1 < 1$ and $c_1 \propto 1/N_T$. These considerations suggest substituting $x_2 = z$ and $x_1 = c_1 z$ in the generic series in (65), which yields the following result.

Lemma 3. *For $x_2 = z$ and $x_1 = c_1 z$, series (65) can be recast as the single infinite series*

$$h(z) = e^{-z} \sum_{n=0}^{\infty} \underbrace{\sum_{m=0}^n \binom{n}{m} \frac{(N)_m}{(N_R + n - m)_m} H_m c_1^m}_{=G_n} \frac{z^n}{n!}. \quad (67)$$

Derivatives of $h(z)$, required below for HGM, are given by

$$\partial_z^k h(z) = \sum_{l=0}^k \binom{k}{l} (-1)^{k-l} e^{-z} \sum_{n=l}^{\infty} G_n \frac{z^{n-l}}{(n-l)!}. \quad (68)$$

Proof: The proof of the first part is not shown, due to simplicity and length limitations. The second part follows from (67) based on Leibniz's formula [38, Eq. (1.4.12), p. 5]. ■

Numerical results shown later reveal that the truncation of (67) still does not converge numerically for practically relevant values of K , N_R , and N_T . Therefore, we shall endeavor to compute it by HGM, as done for Rician-Rayleigh fading in [20] to compute the SNR p.d.f. series deduced from (54). Recall that HGM evaluates a function at given values for its variables by numerically solving its differential equations starting from initial conditions, i.e., known values of the function and required derivatives, at another point [20, Sec. IV.B]. Thus, HGM requires differential equations. Note that, making the substitutions $x_2 = z$ and $x_1 = c_1 z$ and regarding c_1 as a constant factor, conveniently reduces the number of variables in generic series (67). For example, when cast for the m.g.f., the series is only a function of s and z .

Differential equations were derived by hand, with difficulty, for the ZF SNR m.g.f. and p.d.f. in [20, Eqs. (32), (42)] for the Rician-Rayleigh fading case, based on the SNR m.g.f. expression shown here in (52) and the differential equation satisfied by ${}_1F_1(N; N_R; \sigma)$, i.e., [20, Eq. (27)]

$$\begin{aligned} \sigma \cdot {}_1F_1^{(2)}(N; N_R; \sigma) + (N_R - \sigma) \cdot {}_1F_1^{(1)}(N; N_R; \sigma) - \\ N \cdot {}_1F_1(N; N_R; \sigma) = 0. \end{aligned} \quad (69)$$

For the full-Rician fading case with $r = 1$ studied herein, the new SNR m.g.f. expression in (51) comprises an extra sum compared to (52). On the other hand, (67) yields the following complicated SNR m.g.f. expression:

$$M_{\gamma_1}(s; z) = e^{-z} \sum_{n=0}^{\infty} \sum_{m=0}^n \binom{n}{m} \frac{(N)_m M_m(s) c_1^m}{(N_R + n - m)_m} \frac{z^n}{n!}, \quad (70)$$

$$M_m(s) = \sum_{m_1=0}^m \binom{m}{m_1} (-1)^{m_1} \frac{1}{(1 - s\Gamma_1)^{N+m-m_1}}. \quad (71)$$

Because the by-hand derivation of differential equations w.r.t. s and z satisfied by $M_{\gamma_1}(s; z)$ described by (51) or (70) is not tractable, we shall apply instead the automated approach described below, based on the generic expression (67). The derivation of differential equations satisfied by $p_{\gamma_1}(t; z)$, $P_o(z)$, and $C(z)$ can also be automated, based on: 1) their generic expression (67); or 2)

the Laplace-transform relationship between $M_{\gamma_1}(s; z)$ and $p_{\gamma_1}(t; z)$, and the integral relationships of $p_{\gamma_1}(t; z)$ with $P_o(z)$ and $C(z)$. We shall employ the latter approach because it is more general.

V. COMPUTER-ALGEBRA-AIDED DERIVATION OF DIFFERENTIAL EQUATIONS FOR HGM

A. Holonomic Functions, Annihilator, Gröbner Basis, and Creative Telescoping

A function is *holonomic* w.r.t. a set of continuous variables if it satisfies for each of them a linear differential equation with polynomial coefficients. A function is holonomic w.r.t. to a set of discrete variables if the associated generating function is holonomic in the previous sense [20, Sec. IV.C] [30, p. 17]. For example, ${}_1F_1(N; N_R; \sigma)$ is holonomic w.r.t. σ because it satisfies differential equation⁹ (69). In other words, ${}_1F_1(N; N_R; \sigma)$ is *annihilated* by the differential operator $\sigma \partial_\sigma^2 + (N_R - \sigma) \partial_\sigma - N$. The (infinite) set of all operators that annihilate a given holonomic function is called its *annihilator* [30, p. 18].

Holonomic functions are closed under addition, multiplication, certain substitutions, and taking sums and integrals [20], [30]. Consequently, functions $M_{\gamma_1}(s; z)$, $p_{\gamma_1}(t; z)$, $P_o(z)$, and $C(z)$, cast as in (67), are holonomic. The fact that the closure properties for holonomic functions can be executed algorithmically provides a systematic way of deriving the differential equations required for HGM, by starting with the annihilating operators of the comprised “elementary” holonomic functions in (67). A key ingredient for algorithmically executing closure properties is the algebraic concept of *Gröbner basis*, which provides a canonical and finite representation of an annihilator and helps decide whether an operator is in an annihilator. For details on *Gröbner bases* theory, computation, and applications see [32], [30], [34], [35], [33] and references therein.

While many holonomic closure properties require, basically, only linear algebra, computing the annihilator for a sum or integral of a holonomic function is a more involved task. For example, one can employ the *creative telescoping* technique: given an integral $F(x) = \int_a^b f(x, y) dy$, creative telescoping algorithmically finds in the annihilator of $f(x, y)$ a differential operator of the form $P(x, \partial_x) + \partial_y \cdot Q(x, y, \partial_x, \partial_y)$. Then, using the fundamental theorem of calculus [38, p. 6] and differentiating under the integral sign reveals¹⁰ $P(x, \partial_x)$ as an annihilating operator for $F(x)$ [30, p. 46]. Several creative telescoping algorithms are described in [30, Ch. 3].

⁹Note that ${}_1F_1(N; N_R; \sigma)$ is also holonomic w.r.t. N and N_R .

¹⁰Under “natural boundary” conditions [30].

B. The *HolonomicFunctions* Computer-Algebra Package

This freely-available computer-algebra package, written earlier in *Mathematica* by one of the authors, is described, with numerous examples, in [31]. Its commands implement: 1) the computation of Gröbner bases in operator algebras, 2) closure properties for holonomic functions, and 3) creative telescoping algorithms from [30, Ch. 3]. Thus, it enables automated deduction of differential equations for holonomic functions (e.g., our m.g.f. infinite series), their Laplace transform (e.g., our p.d.f.), and their integrals (e.g., our outage probability and ergodic capacity). Conveniently, its symbolic-computation ability¹¹ allows for parameters (e.g., N_R , N , Γ_1 , τ , c_1).

C. Computer-Algebra-Aided Derivation

The *Mathematica* file with *HolonomicFunctions* commands that produce the output discussed and employed below can be downloaded from [36]. Therein, for example, Gröbner basis computation with the command *Annihilator* yields annihilating operators for expression $e^{-z} \frac{z^n}{n!}$ from (67). Further, the command *CreativeTelescoping* yields annihilating operators for G_n based on its definition as the inner sum in (67), and for $P_o(z)$ based on the integral in (59).

Note that the particular functions that enter the differential equations shown below — i.e., $M_{\gamma_1}(s; z)$, $\partial_s M_{\gamma_1}(s; z)$, $\partial_z M_{\gamma_1}(s; z)$; $p_{\gamma_1}(t; z)$, $\partial_t p_{\gamma_1}(t; z)$, $\partial_z p_{\gamma_1}(t; z)$, $\partial_z^2 p_{\gamma_1}(t; z)$; $\partial_z^k P_o(z)$, $k = 0 : 4$; $\partial_z^k C(z)$, $k = 0 : 6$ — arise automatically from (67) by Gröbner basis computation and creative telescoping, and are revealed with the command *UnderTheStaircase* in [36].

The steps and outcomes of the procedure implemented by the code in [36] are as follows:

- 1) Derive SNR m.g.f. differential equations w.r.t. s and z , based on (67). Then, [36] reveals that the function vector

$$\mathbf{m}(s; z) = (M_{\gamma_1}(s; z) \quad \partial_s M_{\gamma_1}(s; z) \quad \partial_z M_{\gamma_1}(s; z))^T$$

satisfies the systems of differential equations w.r.t. s and z

$$\partial_s \mathbf{m}(s; z) = \mathbf{\Theta}_s \mathbf{m}(s; z), \quad \partial_z \mathbf{m}(s; z) = \mathbf{\Theta}_z \mathbf{m}(s; z), \quad (72)$$

with the 3×3 matrices $\mathbf{\Theta}_s$ and $\mathbf{\Theta}_z$ shown only in [36], due to space limitations.

¹¹Inherited from *Mathematica*.

- 2) Using results from Step 1, derive p.d.f. differential equations w.r.t. t and z , based on the inverse-Laplace transform. Then, [36] reveals that the function vector

$$\mathbf{p}(t; z) = (p_{\gamma_1}(t; z) \ \partial_t p_{\gamma_1}(t; z) \ \partial_z p_{\gamma_1}(t; z) \ \partial_z^2 p_{\gamma_1}(t; z))^T$$

satisfies the systems of differential equations w.r.t. t and z

$$\partial_t \mathbf{p}(t; z) = \mathbf{\Xi}_t \mathbf{p}(t; z), \quad \partial_z \mathbf{p}(t; z) = \mathbf{\Xi}_z \mathbf{p}(t; z), \quad (73)$$

with the 4×4 matrices $\mathbf{\Xi}_t$ and $\mathbf{\Xi}_z$ shown in [36].

- 3) Using results from Step 2, derive differential equations w.r.t. z for $P_o(z)$ and $C(z)$, based on their integral relationships from (59) and (61) with $p_{\gamma_1}(t; z)$. Then, [36] reveals that the function vectors $\mathbf{p}_o(z) \doteq 5 \times 1$ with $[\mathbf{p}_o(z)]_k = \partial_z^k P_o(z)$, $k = 0 : 4$, and $\mathbf{c}(z) \doteq 7 \times 1$ with $[\mathbf{c}(z)]_k = \partial_z^k C(z)$, $k = 0 : 6$, satisfy the systems of differential equations

$$\partial_z \mathbf{p}_o(z) = \mathbf{\Phi}_z \mathbf{p}_o(z), \quad \partial_z \mathbf{c}(z) = \mathbf{\Psi}_z \mathbf{c}(z), \quad (74)$$

where $\mathbf{\Phi}_z \doteq 5 \times 5$ and $\mathbf{\Psi}_z \doteq 7 \times 7$ are companion matrices [37, p. 109] shown in [36]. The above systems of differential equations enable the HGM-based computation of the SNR p.d.f., outage probability, and ergodic capacity, as shown below.

VI. NUMERICAL RESULTS

A. Description of Parameter Settings and Approaches

For the channel-matrix mean in (9), unit-norm vector \mathbf{a} and vector \mathbf{b} with the norm in (10) are constructed, according to [1, Eq. (7.29), p. 299], from array response vectors¹², as

$$\mathbf{a} = \frac{1}{\sqrt{N_R}} (1 \ e^{-j\pi \cos(\theta_R)} \ \dots \ e^{-j\pi(N_R-1) \cos(\theta_R)})^T, \quad (75)$$

$$\begin{aligned} \mathbf{b} &= \frac{1}{\sqrt{N_T}} (1 \ e^{-j\pi \cos(\theta_T)} \ \dots \ e^{-j\pi(N_T-1) \cos(\theta_T)})^T \\ &\quad \times \sqrt{\frac{K}{K+1}} N_R N_T, \end{aligned} \quad (76)$$

assuming uniform linear antenna arrays with interelement spacing of half of the carrier wavelength. Above, θ_R and θ_T are, respectively, the angles of arrival and departure of the LoS component w.r.t. the antenna broadside directions. Unless stated otherwise, we assume $\theta_R = 30^\circ$

¹²See [1, Fig. 7.3b, p. 296, Eq. (7.20), p. 297] for geometry and derivation details.

and θ_T equal to the central angle, θ_c , of the transmit-side Laplacian power azimuth spectrum [23, Eq. (4.2)]. Correlation matrix \mathbf{R}_T is computed from the AS and θ_c with [23, Eqs. (4-3)–(4-5)].

Section VI-B below shows results for the Stream-1 outage probability for $\tau = 8.2$ dB, which corresponds to a symbol error probability of 10^{-2} for QPSK modulation. Thus, the constellation size is $M = 4$, and we show P_o vs. $\Gamma_b = \Gamma_s / \log_2 M = \Gamma_s / 2$. On the other hand, Section VI-C shows results for the sum rate, i.e., the sum of the ergodic capacities of all streams, in bits per channel use (bpcu), vs. AS, K , and θ_T . Also shown are simulation results for maximum-likelihood detection (ML).

Unless stated otherwise, presented results have been obtained by running MATLAB R2012a, in its native fixed precision, on a computer with a 3.4-GHz, 64-bit, quad-core¹³ processor and 8 GB of memory. For the simulation results (in figure legends: *Sim.*) we have employed, when feasible, $N_s = 10^6$ samples of \mathbf{n} and \mathbf{H} for (4), to produce reliable results for P_o as low as 10^{-5} . Then, series results (in legends: *Series*) have been produced by truncating (67) as in [19, Section V.F], i.e., new terms have been added until: 1) their relative change falls below 10^{-10} , or 2) $n \leq n_{\max} = 150$, as additional terms in (67) lead to numerical divergence because the arising large numbers are represented with poor precision. Numerical divergence is indicated in legends with *Series**. Outage probability results for full-Rayleigh fading (in legend: *Rayleigh, Exp.*) have been obtained with expression $P_o = \frac{\gamma(N, \tau/\Gamma_1)}{(N-1)!}$, obtained from (60) based on Remark 5. Finally, HGM results (in legends: *HGM*) have been produced by solving — with the MATLAB `ode45` function with tolerance levels of 10^{-10} — the systems of differential equations in (74). Then, for the outage probability, the initial condition $\mathbf{p}_o(z_0)$ has been computed accurately with (67) and (68) at $z_0 = 0.05692$, which arises from (41) for $K = -25$ dB, $N_R = 6$, $N_T = 4$, and $\mathbf{R}_T = \mathbf{I}_{N_T}$. Finally, sum rate results have been obtained by adding the ergodic capacities of the N_T streams.

Results are shown for K and AS values relevant to their lognormal distributions for WINNER II scenarios A1 (indoors office) and C2 (urban macrocell), under LoS propagation [22, Table 5.5]: 1) averages of these distributions, i.e., for $K = 7$ dB, and for AS = 51° and 11° , which yield low and high antenna element correlation, i.e., $|\mathbf{R}_T]_{1,2}| = 0.12$ and 0.83 , respectively; 2) values

¹³Nevertheless, we have run single instances of MATLAB when measuring the computation time (with `tic`, `toc`.)

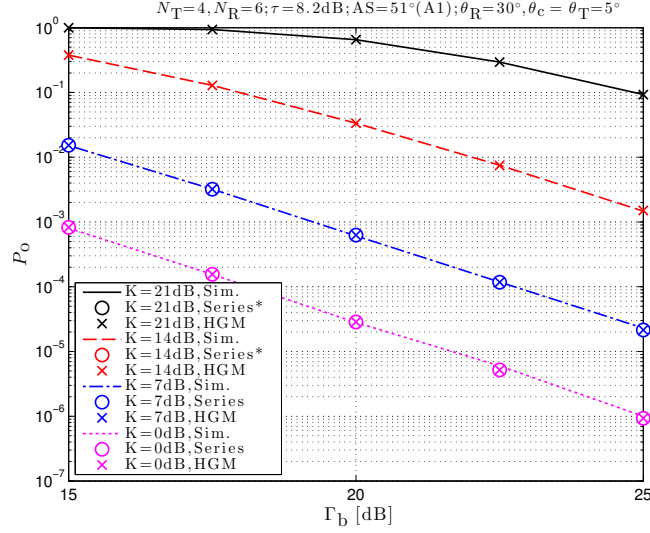


Fig. 1. Stream-1 outage probability for $N_R = 6$, $N_T = 4$, $\text{AS} = 51^\circ$ (i.e., scenario A1 mean), and various values of K , including $K = 7$ dB (i.e., scenario A1 mean). Series results for $K = 14, 21$ dB do not appear because of numerical divergence.

within the range of most likely values [18, Table 1], or 3) random samples¹⁴.

B. Outage Probability Results

1) Description of Results for K and AS Relevant to Scenario A1, and for Small N_R and N_T :

Fig. 1 shows results for $\text{AS} = 51^\circ$ and K set to values from 0 dB to the upper limit of the range expected with 0.99 probability for scenario A1 [18, Table 1]. Note that the MATLAB series truncation diverges for $K = 14$ dB and 21 dB¹⁵, whereas HGM and simulation results agree at all K . Thus, HGM enables us to investigate the performance degradation likely to occur in practice with increasing K for MIMO ZF under full-Rician fading with $r = 1$.

Fig. 2 shows results from averaging also over AS and K from their WINNER II lognormal distributions for scenario A1. First, simulation has not been attempted due to the long required time. (The computation time is explored in more detail below.) Series truncation does not yield useful results because of numerical divergence for the larger K values. Only HGM has yielded

¹⁴Then, even computing \mathbf{R}_T with [23, Eqs. (4-3)–(4-5)] is time consuming; nevertheless, the employed 2,100 samples of AS and K have yielded smooth outage probability plots.

¹⁵Our series truncation in Mathematica, with its arbitrary precision, converged also for $K = 14$ dB, but required one hour vs. a few seconds for HGM; series truncation in Mathematica was not tried for $K = 21$ dB.

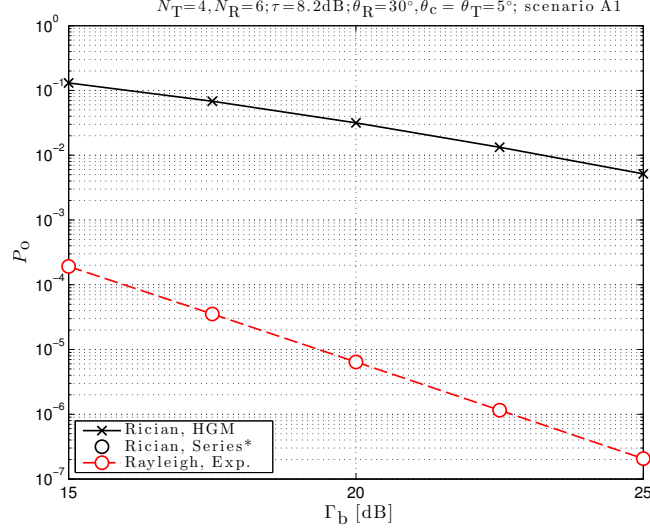


Fig. 2. Stream-1 outage probability for $N_R = 6$, $N_T = 4$, averaged also over the WINNER II lognormal distributions of K and AS for scenario A1. Results corresponding to Rician, Series do not appear because of numerical divergence.

relatively expeditiously a smooth plot whose unshown continuation at sufficiently large Γ_b has revealed the expected diversity order¹⁶ of $N = 3$ [19, Eq. (46)].

Figs. 1 and 2 depict the same Γ_b range in order to reveal that: 1) setting AS and K to their averages can substantially overestimate performance vs. averaging over AS and K — compare the blue dash-dotted plot in Fig. 1 with the solid black plot in Fig. 2; 2) making the assumption of full-Rayleigh fading instead of full-Rician fading leads to unrealistic performance expectations — compare the plots in Fig. 2.

2) *Description of Results for K , AS Relevant to Scenarios A1, C2, and for Increasing N_R , N_T :*

Table I summarizes results of several numerical experiments for K and AS set to their averages for scenarios A1 and C2, and for the pair (N_R, N_T) set to $N_a \times (6, 4)$, with N_a shown in the second column¹⁷. The Γ_b ranges shown in the third column yield P_o in the order of $10^{-2} - 10^{-5}$, as shown in the fourth column. The remaining three columns show the actual or estimated computation

¹⁶The expected diversity order is also noticeable from the plots for $K = 0$ dB and 7 dB in Fig. 1.

¹⁷Note that N_R does not necessarily have to be much larger than N_T even in massive MIMO [7].

TABLE I

RESULTS FOR $K = 7$ dB, AS = 51° (I.E., SCENARIO A1) AND AS = 11° (C2), AND $(N_R, N_T) = N_a \times (6, 4)$.

AS	N_a	Γ_b (dB)	$P_o = [a \times 10^{-2}, b \times 10^{-5}]$	Series	Sim. ($N_s = 10^6$)	HGM
51° (A1)	1	[15, 25]	$a = 1.53, b = 2.15$	1.3 s ✓	31 s	20 s ✓
51° (A1)	2	[11, 17]	$a = 1.74, b = 4.26$	1.3 s ✗	53 s	20 s ✓
51° (A1)	5	[6, 9]	$a = 1.39, b = 6.39$	1.3 s ✗	520 s	20 s ✓
51° (A1)	10	[2, 4.5]	$a = 2.35, b = 2.45$	1.3 s ✗	2,300 s	20 s ✓
51° (A1)	15	[0, 2]	$a = 1.98, b = 1.61$	1.3 s ✗	8,800 s	20 s ✓
51° (A1)	100	[-9.2, -8.5]	$a = 2.72, b = 2.57$	1.3 s ✗	<i>estimated</i> : 1.9×10^6 s ✗	20 s ✓
11° (C2)	1	[23, 32]	$a = 1.12, b = 3.01$	1.3 s ✓	31 s	20 s ✓
11° (C2)	2	[18.5, 24.5]	$a = 1.43, b = 3.36$	1.3 s ✗	54 s	20 s ✓
11° (C2)	10	[5, 7.5]	$a = 2.12, b = 2.09$	1.3 s ✗	2,400 s	20 s ✓

time (in seconds), per Γ_b value. The marks ✓ and ✗ in the ‘Series’ column denote, respectively, successful and unsuccessful (i.e., numerical divergence) series computation¹⁸. Further, mark ✗ in the ‘Sim.’ column indicates infeasible simulation duration. Finally, mark ✓ in the ‘HGM’ column indicates successful HGM-based computation. This table demonstrates that, unlike series truncation and simulation, HGM enables reliable, accurate, and expeditious ZF assessments for realistic K and even large MIMO.

Fig. 3 characterizes ZF performance for $K = 7$ dB and AS = 51° , and for the large-MIMO setting with $N_R = 100$ and $N_T = 20$. On the one hand, series truncation does not produce useful results; on the other hand, HGM results agree with the simulation results, and we have found HGM over 30 times faster¹⁹.

C. Ergodic Capacity Results

The ZF ergodic capacity has been computed, for each stream, for $N_R = 6$, $N_T = 4$, $\theta_c = 5^\circ$, and $\Gamma_s = 10$ dB by: 1) HGM based on (74) with Ψ_z shown in [36], 2) simulation (also for ML), and 3) the infinite series in (67). Results from the series do not appear in the figures because, as for the outage probability, its truncation diverges for realistic values of K .

Fig. 4 demonstrates that increasing AS (decreasing antenna correlation) yields increasing ZF sum rate and decreasing ML–ZF rate gap. On the other hand, Fig. 5 reveals that increasing K

¹⁸For $(N_R = 6, N_T = 4)$ numerical convergence is achieved with $n = 134$, whereas the other (N_R, N_T) pairs yield $n = n_{\max} = 150$. Consequently, MATLAB reports about the same computation time (≈ 1.3 s) for all cases.

¹⁹When large N_T yields infeasibly-long simulation, HGM results can be validated by checking the diversity order revealed by its P_o -vs.- Γ_b plot. E.g., for $N_R = 104$ and $N_T = 100$, we have found its slope magnitude to be near the expected $N = 5$.

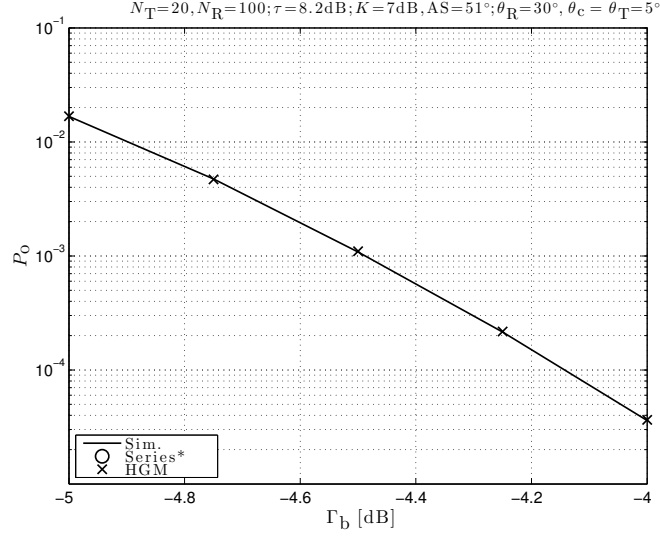


Fig. 3. Stream-1 outage probability for $N_R = 100$, $N_T = 20$, for $K = 7$ dB and $AS = 51^\circ$ (i.e., averages for scenario A1). Results corresponding to *Series* do not appear because of numerical divergence.

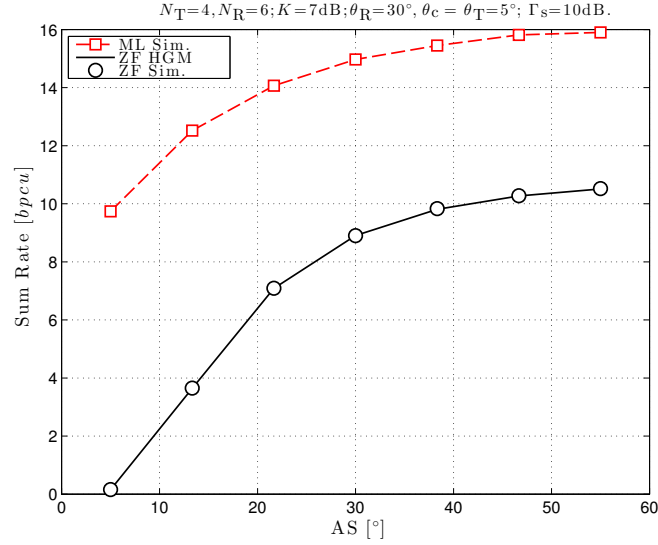


Fig. 4. ZF sum rate from HGM and simulation vs. AS , for $N_R = 6$, $N_R = 4$, $K = 7$ dB; also, ML sum rate from simulation.

yields decreasing ZF sum rate and increasing ML–ZF rate gap, for large AS (e.g., 51°). However, other (unshown) results indicate that the ML–ZF gap is decreasing for small AS (e.g., 7°) and is constant for medium AS (e.g., 12°).

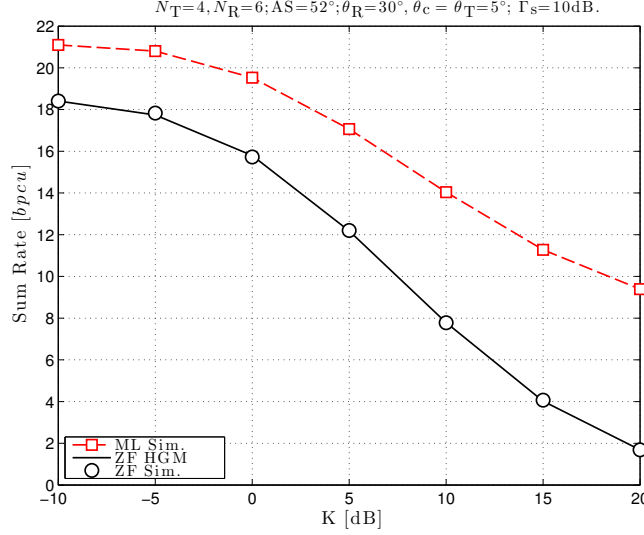


Fig. 5. ZF sum rate from HGM and simulation vs. K , for $N_R = 6$, $N_T = 4$, $AS = 52^\circ$; also, ML sum rate from simulation.

Finally, Fig. 6 reveals, for $AS = 12^\circ$ and $\theta_c = 5^\circ$, a substantial sum rate decrease with decreasing $|\theta_T - \theta_c|$. Based on Remark 7, because condition $\theta_T = \theta_c$ yields worst performance, it must also minimize $\|\mathbf{h}_{d,1} - \mathbf{H}_{d,2}\mathbf{r}_{2,1}\|$. For larger AS , other (unshown) results have revealed more moderate rate gain with increasing $|\theta_T - \theta_c|$. For very large AS (e.g., 51°), the sum rate remains unchanged with increasing $|\theta_T - \theta_c|$, because large AS yields $\mathbf{r}_{2,1} \approx \mathbf{0}$, i.e., $\|\mathbf{h}_{d,1} - \mathbf{H}_{d,2}\mathbf{r}_{2,1}\| \approx \|\mathbf{h}_{d,1}\|$, which is independent of $|\theta_T - \theta_c|$. Unshown numerical results from the approximating gamma distribution from Remark 6 have revealed it inaccurate especially for small N_R , N_T , and K . On the other hand, we have found that accuracy improves with smaller $|\theta_T - \theta_c|$, which corroborates Remark 7.

VII. SUMMARY, CONCLUSIONS, AND FUTURE WORK

This paper has provided an exact performance analysis and evaluation of MIMO spatial multiplexing with ZF, under transmit-correlated full-Rician fading with LoS component of rank $r = 1$. First, we expressed as infinite series the SNR m.g.f. and p.d.f., as well as performance measures, e.g., the outage probability and ergodic capacity. However, their numerical convergence has been revealed inherently more problematic with increasing K , N_R , and N_T . Therefore, we have applied computer algebra to the derived infinite series and deduced satisfied differential

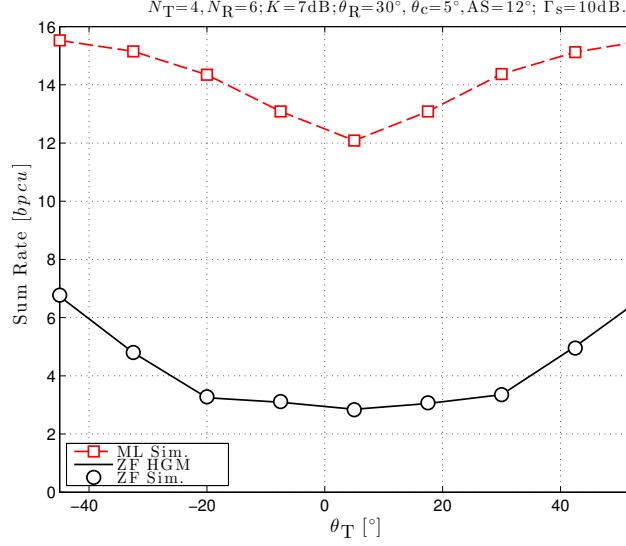


Fig. 6. Sum rate vs. θ_T for $\theta_c = 5^\circ$, when $N_R = 6$, $N_R = 4$, $K = 7$ dB, $AS = 12^\circ$; also, ML sum rate from simulation.

equations. They have been used for HGM-based computation. Thus, we have expeditiously produced accurate results for the range of realistic values of K and even for large N_R and N_T . Consequently, we have been able to assess the substantial performance degradation incurred with increasing K for ZF when $r = 1$. Furthermore, HGM has helped reveal that the performance averaged over WINNER II AS and K distributions can be much worse than that for average AS and K . Finally, we have been able to evaluate the performance for antenna numbers relevant to large MIMO reliably and much more expeditiously than by simulation.

Based on our experience studying MIMO for Rician fading for ZF in this paper and for MRC²⁰ in our ongoing work, we expect that performance measure expressions for larger r and other transceiver techniques shall entail multiple infinite series in factors proportional to K , N_R and N_T , which shall diverge numerically for realistic values of these parameters. Alternate computation with the HGM shall require differential equations. Because their by-hand derivation from the infinite series shall be intractable, computer algebra shall be indispensable.

²⁰Here, MRC refers to the MIMO technique of transmitting and receiving over the dominant channel mode, as discussed in [40].

APPENDIX

A. Proof of Lemma 1

Based on (39) and (42), we can regard $[\mathbf{G}_2]_{\bullet,1} \doteq N_R \times 1$, as a vector of independent complex-valued Gaussians with variance of $1/2$ for the real and imaginary parts, and means

$$\mathbb{E}\{[\mathbf{G}_2]_{1,1}\} = \sqrt{x_2}, \quad \mathbb{E}\{[\mathbf{G}_2]_{i,1}\} = 0, \quad i = 2 : N_R, \quad (77)$$

which yield

$$\frac{|[\mathbf{G}_2]_{1,1}|^2}{1/2} \sim \chi_2^2 \left(\frac{x_2}{1/2} \right), \quad (78)$$

$$\frac{|[\mathbf{G}_2]_{2,1}|^2}{1/2} + \dots + \frac{|[\mathbf{G}_2]_{N_R,1}|^2}{1/2} \sim \chi_{2(N_R-1)}^2. \quad (79)$$

Now, because \mathbf{T}_2 in (44) is upper triangular, we can write the first column of $\mathbf{G}_2 = \mathbf{U}_2 \mathbf{T}_2$ as $[\mathbf{G}_2]_{\bullet,1} = [\mathbf{U}_2]_{\bullet,1} [\mathbf{T}_2]_{11}$. If we set

$$[\mathbf{T}_2]_{1,1} = \|[\mathbf{G}_2]_{\bullet,1}\|, \quad [\mathbf{U}_2]_{\bullet,1} = \frac{[\mathbf{G}_2]_{\bullet,1}}{\|[\mathbf{G}_2]_{\bullet,1}\|}, \quad (80)$$

then

$$|[\mathbf{U}_2]_{1,1}|^2 = \frac{|[\mathbf{G}_2]_{1,1}|^2}{|[\mathbf{G}_2]_{1,1}|^2 + |[\mathbf{G}_2]_{2,1}|^2 + \dots + |[\mathbf{G}_2]_{N_R,1}|^2}. \quad (81)$$

Finally, using (78), (79), and the independence of $[\mathbf{G}_2]_{i,1}$, $i = 1 : N_R$, one can show that [41]

$$\begin{aligned} |[\mathbf{U}_2]_{1,1}|^2 &\sim \text{B}(1, N_R - 1, 2x_2), \\ \beta_1 &\stackrel{(46)}{=} 1 - |[\mathbf{U}_2]_{1,1}|^2 \sim \text{B}(N_R - 1, 1, 2x_2). \end{aligned}$$

The p.d.f. of β_1 is then given by [41]

$$f_{\beta_1}(v) = \sum_{n_2=0}^{\infty} \frac{e^{-x_2} x_2^{n_2}}{n_2!} \underbrace{\left(\frac{v^{(N_R-1)-1} (1-v)^{(n_2+1)-1}}{\int_0^1 t^{(N_R-1)-1} (1-t)^{(n_2+1)-1} dt} \right)}_{=f_{\beta_3}(v; N_R-1, n_2+1)}, \quad (82)$$

where $f_{\beta_3}(v; N_R - 1, n_2 + 1)$ is the p.d.f. of a variable $\beta_3 \sim \text{B}(N_R - 1, n_2 + 1)$. Then, the n_1 th moment of β_1 is

$$\begin{aligned} \mathbb{E}\{\beta_1^{n_1}\} &= \sum_{n_2=0}^{\infty} \frac{e^{-x_2} x_2^{n_2}}{n_2!} \mathbb{E}\{\beta_3^{n_1}\} \\ &= \sum_{n_2=0}^{\infty} \frac{e^{-x_2} x_2^{n_2}}{n_2!} \frac{(N_R - 1)_{n_1}}{(n_2 + N_R)_{n_1}}. \end{aligned} \quad (83)$$

B. Proof of Lemma 2

First, let us consider the $N_R \times N_R$ matrix $\hat{\mathbf{G}}_2 = (\mathbf{G}_2 \quad \tilde{\mathbf{G}}_2) \sim \mathcal{CN}_{N_R, N_R}(\hat{\mathbf{G}}_{d,2}, \mathbf{I}_{N_R} \otimes \mathbf{I}_{N_R})$ obtained by joining the $N_R \times N_I$ matrix $\mathbf{G}_2 \sim \mathcal{CN}_{N_R, N_I}(\mathbf{G}_{d,2}, \mathbf{I}_{N_R} \otimes \mathbf{I}_{N_I})$ from (39) — whose sole nonzero-mean column is $[\mathbf{G}_2]_{\bullet,1}$ — with the $N_R \times N$ matrix $\tilde{\mathbf{G}}_2 \sim \mathcal{CN}_{N_R, N}(\mathbf{0}, \mathbf{I}_{N_R} \otimes \mathbf{I}_N)$. Then, paralleling (44), let us consider its QR decomposition, i.e.,

$$\hat{\mathbf{G}}_2 = (\mathbf{G}_2 \quad \tilde{\mathbf{G}}_2) = \hat{\mathbf{U}}_2 \hat{\mathbf{T}}_2, \quad (84)$$

with $\hat{\mathbf{U}}_2 \doteq N_R \times N_R$ unitary, i.e., $\hat{\mathbf{U}}_2^H \hat{\mathbf{U}}_2 = \hat{\mathbf{U}}_2 \hat{\mathbf{U}}_2^H = \mathbf{I}_{N_R}$, and $\hat{\mathbf{T}}_2 \doteq N_R \times N_R$ upper triangular with positive diagonal elements. By partitioning in (84) and using (44), we can write

$$\begin{aligned} \hat{\mathbf{G}}_2 &= (\mathbf{G}_2 \quad \tilde{\mathbf{G}}_2) = (\mathbf{U}_2 \quad \tilde{\mathbf{U}}_2) \begin{pmatrix} \mathbf{T}_2 & \tilde{\mathbf{T}}_{12} \\ \mathbf{0} & \tilde{\mathbf{T}}_{22} \end{pmatrix} \\ &= (\mathbf{U}_2 \mathbf{T}_2 \quad \mathbf{U}_2 \tilde{\mathbf{T}}_{12} + \tilde{\mathbf{U}}_2 \tilde{\mathbf{T}}_{22}), \end{aligned} \quad (85)$$

where $\tilde{\mathbf{U}}_2 \doteq N_R \times N$ satisfies $\tilde{\mathbf{U}}_2^H \tilde{\mathbf{U}}_2 = \mathbf{I}_N$, $\tilde{\mathbf{T}}_{12} \doteq N_I \times N$, and $\tilde{\mathbf{T}}_{22} \doteq N \times N$ is upper triangular with positive diagonal elements.

Hereafter, let us assume that $[\mathbf{G}_2]_{\bullet,1}$ is given, i.e., $[\mathbf{U}_2]_{\bullet,1}$ set as in (80) is given. Then, the distribution of

$$\begin{aligned} \hat{\mathbf{G}}_2 &\stackrel{(84)}{=} \hat{\mathbf{U}}_2 \hat{\mathbf{T}}_2 = (\mathbf{U}_2 \quad \tilde{\mathbf{U}}_2) \hat{\mathbf{T}}_2 \\ &= ([\mathbf{U}_2]_{\bullet,1} \quad [\mathbf{U}_2]_{\bullet,2} \quad \dots \quad [\mathbf{U}_2]_{\bullet, N_I} \quad \tilde{\mathbf{U}}_2) \hat{\mathbf{T}}_2 \end{aligned}$$

is invariant to unitary transformations of the columns $[\mathbf{U}_2]_{\bullet,i}$, $\forall i = 2 : N_I$ and the columns of $\tilde{\mathbf{U}}_2$. Thus, we may rewrite

$$\hat{\mathbf{U}}_2 = (\mathbf{U}_2 \quad \tilde{\mathbf{U}}_2) = ([\mathbf{U}_2]_{\bullet,1} \quad \mathbf{U}^0 \mathbf{P}), \quad (86)$$

where $\mathbf{U}^0 \doteq N_R \times (N_R - 1)$ comprises fixed orthonormal vectors selected to form a basis with $[\mathbf{U}_2]_{\bullet,1}$, and $\mathbf{P} \doteq (N_R - 1) \times (N_R - 1)$ is unitary, Haar-distributed [19, Sec. III.E], not dependent on $[\mathbf{U}_2]_{\bullet,1}$. Using the first row of \mathbf{U}^0 to define

$$\mathbf{q}^T = [\mathbf{U}^0]_{1,\bullet} \cdot \mathbf{P} \doteq 1 \times (N_R - 1), \quad (87)$$

the first row of $\hat{\mathbf{U}}_2$ from (86) can be written as

$$[\hat{\mathbf{U}}_2]_{1,\bullet} = ([\mathbf{U}_2]_{1,1} \quad \mathbf{q}^T). \quad (88)$$

Then, based on $\widehat{\mathbf{U}}_2 \widehat{\mathbf{U}}_2^H = \mathbf{I}_{N_R}$ and (88), we can write

$$\begin{aligned} 1 &= \|[\widehat{\mathbf{U}}_2]_{1,\bullet}\|^2 = |[\mathbf{U}_2]_{1,1}|^2 + \|\mathbf{q}\|^2 \Rightarrow \\ \|\mathbf{q}\|^2 &= 1 - |[\mathbf{U}_2]_{1,1}|^2. \end{aligned} \quad (89)$$

From (87) and (89) we deduce that the vector

$$\frac{\mathbf{q}}{\|\mathbf{q}\|} = \frac{\mathbf{q}}{\sqrt{1 - |[\mathbf{U}_2]_{1,1}|^2}} \quad (90)$$

is uniformly distributed on the unit sphere \mathbb{S}^{N_R-2} .

Finally, because we can write

$$\begin{aligned} [\widehat{\mathbf{U}}_2]_{1,\bullet} &\stackrel{(86)}{=} ([\mathbf{U}_2]_{1,1} \quad [\mathbf{U}_2]_{1,2} \quad \dots \quad [\mathbf{U}_2]_{1,N_I} \quad [\widetilde{\mathbf{U}}_2]_{1,\bullet}) \\ &\stackrel{(88)}{=} ([\mathbf{U}_2]_{1,1} \quad q_1 \quad \dots \quad q_{N_I-1} \quad q_{N_I} \quad \dots \quad q_{N_R-1}), \end{aligned}$$

we have that $[\mathbf{U}_2]_{1,2}, \dots, [\mathbf{U}_2]_{1,N_I}$ are the first $N_I - 1$ elements of \mathbf{q} . Thus, we can write, by also using (89),

$$\begin{aligned} \beta_4 &= \frac{|[\mathbf{U}_2]_{1,2}|^2 + \dots + |[\mathbf{U}_2]_{1,N_I}|^2}{1 - |[\mathbf{U}_2]_{1,1}|^2} \\ &= \frac{|q_1|^2 + \dots + |q_{N_I-1}|^2}{(|q_1|^2 + \dots + |q_{N_I-1}|^2) + (|q_{N_I}|^2 + \dots + |q_{N_R-1}|^2)}. \end{aligned}$$

Recalling that $\frac{\mathbf{q}}{\|\mathbf{q}\|}$ is uniformly distributed, we can deduce that, conditioned on $[\mathbf{G}_2]_{\bullet,1}$, i.e., on $[\mathbf{U}_2]_{\bullet,1}$, random variables β_4 and $\beta_2 \stackrel{(46)}{=} 1 - \beta_4$ have the following distributions [41]:

$$\begin{aligned} \beta_4 &\sim \mathbf{B}(N_I - 1, N_R - N_I) = \mathbf{B}(N_T - 2, N), \\ \beta_2 = 1 - \beta_4 &\sim \mathbf{B}(N_R - N_I, N_I - 1) = \mathbf{B}(N, N_T - 2). \end{aligned}$$

Because the distribution of β_2 does not depend on $[\mathbf{U}_2]_{\bullet,1}$, we also deduce that β_2 is independent of $\beta_1 \stackrel{(46)}{=} 1 - |[\mathbf{U}_2]_{1,1}|^2$.

C. Derivation of Expressions for x_1 and x_2

From Remark 1, the normalized vector $\mathbf{b}_n = \frac{\mathbf{b}}{\|\mathbf{b}\|} \doteq N_T \times 1$ does not depend on K . Defining

$$\widetilde{\mathbf{R}} = \begin{pmatrix} 0 & \mathbf{0} \\ \mathbf{0} & \mathbf{R}_{T,K_{22}}^{-1} \end{pmatrix} \doteq N_T \times N_T, \quad (91)$$

$$\widetilde{\mathbf{r}}_{2,1} = (1 \quad -\mathbf{r}_{2,1}^T)^T \doteq N_T \times 1, \quad (92)$$

we can write μ_1 from (28) and $\tilde{\mathbf{b}}^H \mathbf{R}_{T,K_{22}}^{-1} \tilde{\mathbf{b}}$ from (41) as:

$$\mu_1 = b_1^* - \tilde{\mathbf{b}}^H \mathbf{r}_{2,1} = \mathbf{b}^H \tilde{\mathbf{r}}_{2,1} = \|\mathbf{b}\| \mathbf{b}_n^H \tilde{\mathbf{r}}_{2,1}, \quad (93)$$

$$\tilde{\mathbf{b}}^H \mathbf{R}_{T,K_{22}}^{-1} \tilde{\mathbf{b}} = \mathbf{b}^H \tilde{\mathbf{R}} \mathbf{b} = \|\mathbf{b}\|^2 \mathbf{b}_n^H \tilde{\mathbf{R}} \mathbf{b}_n. \quad (94)$$

Finally, from (10) we have that $\|\mathbf{b}\|^2 = K N_R N_T / (K+1)$. From (11) we have that $[\mathbf{R}_{T,K}^{-1}]_{1,1} \propto (K+1)$ and $\mathbf{R}_{T,K_{22}}^{-1} \propto (K+1)$, i.e., $\tilde{\mathbf{R}} \propto (K+1)$, whereas $\mathbf{r}_{2,1}$ defined in (23), i.e., $\tilde{\mathbf{r}}_{2,1}$ defined in (92), does not depend on K . These yield:

$$x_1 \stackrel{(30)}{=} [\mathbf{R}_{T,K}^{-1}]_{1,1} |\mu_1|^2 \propto K N_R N_T, \quad (95)$$

$$x_2 \stackrel{(41)}{=} \tilde{\mathbf{b}}^H \mathbf{R}_{T,K_{22}}^{-1} \tilde{\mathbf{b}} \propto K N_R N_T. \quad (96)$$

REFERENCES

- [1] D. Tse and P. Viswanath, *Fundamentals of Wireless Communication*. Cambridge, UK: Cambridge University Press, 2005.
- [2] D. Gesbert, M. Kountouris, R. Heath, C.-B. Chae, and T. Salzer, "Shifting the MIMO paradigm," *IEEE Signal Processing Magazine*, vol. 24, no. 5, pp. 36–46, Sep. 2007.
- [3] H. Q. Ngo, M. Matthaiou, T. Duong, and E. Larsson, "Uplink performance analysis of multicell MU-SIMO systems with ZF receivers," *IEEE Transactions on Vehicular Technology*, vol. 62, no. 9, pp. 4471–4483, Nov 2013.
- [4] F. Rusek, D. Persson, B. K. Lau, E. G. Larsson, T. L. Marzetta, O. Edfors, and F. Tufvesson, "Scaling up MIMO: Opportunities and challenges with very large arrays," *IEEE Signal Processing Magazine*, vol. 30, no. 1, pp. 40–60, 2013.
- [5] J. Hoydis, S. ten Brink, and M. Debbah, "Massive MIMO in the UL/DL of cellular networks: How many antennas do we need?" *IEEE Journal on Selected Areas in Communications*, vol. 31, no. 2, pp. 160–171, 2013.
- [6] L. Lu, G. Li, A. Swindlehurst, A. Ashikhmin, and R. Zhang, "An overview of massive MIMO: Benefits and challenges," *IEEE Journal of Selected Topics in Signal Processing*, vol. 8, no. 5, pp. 742–758, Oct 2014.
- [7] E. Björnson, E. G. Larsson, and T. L. Marzetta, "Massive MIMO: Ten myths and one critical question," *IEEE Communications Magazine*, Feb 2016.
- [8] J. H. Winters, J. Salz, and R. D. Gitlin, "The impact of antenna diversity on the capacity of wireless communication systems," *IEEE Transactions on Communications*, vol. 42, no. 234, pp. 1740–1751, 1994.
- [9] D. A. Gore, R. W. Heath, and A. J. Paulraj, "Transmit selection in spatial multiplexing systems," *IEEE Communications Letters*, vol. 6, no. 11, pp. 491–493, 2002.
- [10] M. Kiessling and J. Speidel, "Analytical performance of MIMO zero-forcing receivers in correlated Rayleigh fading environments," in *IEEE Workshop on Signal Proc. Advances in Wireless Comm. (SPAWC'03)*, June 2003, pp. 383–387.
- [11] R. U. Nabar, H. Bolcskei, and A. J. Paulraj, "Diversity and outage performance in space-time block coded Ricean MIMO channels," *IEEE Transactions on Wireless Communications*, vol. 4, no. 5, pp. 2519–2532, Sep 2005.
- [12] M. Kang and M.-S. Alouini, "Capacity of MIMO Rician channels," *IEEE Transactions on Wireless Communications*, vol. 5, no. 1, pp. 112–122, Jan 2006.
- [13] S. Jin, X. Gao, and X. You, "On the ergodic capacity of rank-1 Ricean-fading MIMO channels," *IEEE Transactions on Information Theory*, vol. 53, no. 2, pp. 502–517, Feb. 2007.

- [14] M. McKay, A. Zanella, I. Collings, and M. Chiani, "Error probability and SINR analysis of optimum combining in Rician fading," *IEEE Transactions on Communications*, vol. 57, no. 3, pp. 676–687, Mar 2009.
- [15] M. Matthaiou, C. Zhong, and T. Ratnarajah, "Novel generic bounds on the sum rate of MIMO ZF receivers," *IEEE Transactions on Signal Processing*, vol. 59, no. 9, pp. 4341–4353, Sep 2011.
- [16] J. Li, M. Matthaiou, S. Jin, and T. Svensson, "Energy efficiency analysis of rank-1 Ricean fading MIMO channels," in *IEEE International Workshop on Signal Processing Advances in Wireless Communications (SPAWC'14)*, 2014, pp. 349–353.
- [17] Q. Zhang, S. Jin, K.-K. Wong, H. Zhu, and M. Matthaiou, "Power scaling of uplink massive MIMO systems with arbitrary-rank channel means," *IEEE Journal of Selected Topics in Signal Processing*, vol. 8, no. 5, pp. 966–981, Oct 2014.
- [18] C. Siriteanu, Y. Miyanaga, S. D. Blostein, S. Kuriki, and X. Shi, "MIMO zero-forcing detection analysis for correlated and estimated Rician fading," *IEEE Transactions on Vehicular Technology*, vol. 61, no. 7, pp. 3087–3099, Sep 2012.
- [19] C. Siriteanu, S. D. Blostein, A. Takemura, H. Shin, S. Yousefi, and S. Kuriki, "Exact MIMO zero-forcing detection analysis for transmit-correlated Rician fading," *IEEE Trans. on Wireless Communications*, vol. 13, no. 3, pp. 1514–1527, Mar 2014.
- [20] C. Siriteanu, A. Takemura, S. Kuriki, H. Shin, and C. Koutschan, "MIMO zero-forcing performance evaluation using the holonomic gradient method," *IEEE Transactions on Wireless Communications*, vol. 14, no. 4, pp. 2322–2335, Apr 2015.
- [21] C. Siriteanu, A. Takemura, S. Kuriki, D. Richards, and H. Shin, "Schur complement based analysis of MIMO zero-forcing for Rician fading," *IEEE Transactions on Wireless Communications*, vol. 14, no. 4, pp. 1757–1771, Apr 2015.
- [22] P. Kyosti, J. Meinila, L. Hentila, and *et al.*, "WINNER II Channel Models. Part I," CEC, Tech. Rep. IST-4-027756, 2008.
- [23] C. Siriteanu, "Maximal-ratio eigen-combining for smarter antenna array wireless communication receivers," Ph.D. dissertation, Queen's University, Kingston, Canada, 2006. [Online]. Available: http://post.queensu.ca/~sdb2/PAPERS/thesis_siriteanu.pdf
- [24] E. Torkildson, U. Madhow, and M. Rodwell, "Indoor millimeter wave MIMO: Feasibility and performance," *IEEE Transactions on Wireless Communications*, vol. 10, no. 12, pp. 4150–4160, Dec 2011.
- [25] J. Brady, N. Behdad, and A. M. Sayeed, "Beamspace MIMO for millimeter-wave communications: System architecture, modeling, analysis, and measurements," *IEEE Trans. on Antennas and Propagation*, vol. 61, no. 7, pp. 3814–3827, 2013.
- [26] R. W. Heath Jr, N. Gonzalez-Prelcic, S. Rangan, W. Roh, and A. Sayeed, "An overview of signal processing techniques for millimeter wave MIMO systems," *IEEE Journal on Selected Topics in Signal Processing*, to appear, 2016. [Online]. Available: <http://arxiv.org/abs/1512.03007>
- [27] A. M. Sayeed, "Deconstructing multiantenna fading channels," *IEEE Transactions on Signal Processing*, vol. 50, no. 10, pp. 2563–2579, 2002.
- [28] A. Sayeed and J. Brady, "Beamspace MIMO for high-dimensional multiuser communication at millimeter-wave frequencies," in *Global Communications Conference (GLOBECOM), 2013 IEEE*, 2013, pp. 3679–3684.
- [29] M. Matthaiou, M. McKay, P. Smith, and J. Nossék, "On the condition number distribution of complex Wishart matrices," *IEEE Transactions on Communications*, vol. 58, no. 6, pp. 1705–1717, June 2010.
- [30] C. Koutschan, "Advanced applications of the holonomic systems approach," Ph.D. dissertation, Research Institute for Symbolic Computation (RISC), Johannes Kepler University, Linz, Austria, 2009. [Online]. Available: <http://www.risc.jku.at/research/combinat/software/HolonomicFunctions/>
- [31] —, "HolonomicFunctions (user's guide)," RISC Report Series, Johannes Kepler University, Linz, Austria, Tech. Rep. 10-01, 2010. [Online]. Available: <http://www.risc.jku.at/research/combinat/software/HolonomicFunctions/>
- [32] B. Buchberger, "Bruno Buchberger's PhD thesis 1965: An algorithm for finding the basis elements of the residue class

- ring of a zero dimensional polynomial ideal,” *Journal of Symbolic Computation*, vol. 41, no. 34, pp. 475 – 511, 2006. [Online]. Available: <http://www.sciencedirect.com/science/article/pii/S0747717105001483>
- [33] Z. Lin, L. Xu, and N. K. Bose, “A tutorial on Gröbner bases with applications in signals and systems,” *IEEE Transactions on Circuits and Systems I: Regular Papers*, vol. 55, no. 1, pp. 445–461, 2008.
- [34] Q. Geng, S. Kannan, and P. Viswanath, “Interactive interference alignment,” *IEEE Journal on Selected Areas in Communications*, vol. 32, no. 9, pp. 1699–1706, 2014.
- [35] M. Fozunbal, S. W. McLaughlin, R. W. Schafer, and J. M. Landsberg, “On space-time coding in the presence of spatio-temporal correlation,” *IEEE Transactions on Information Theory*, vol. 50, no. 9, pp. 1910–1926, 2004.
- [36] C. Koutschan. Mathematica notebook Rank1Rice.nb with derivations of differential equations using the HolonomicFunctions package. [Online]. Available: <http://www.koutschan.de/data/rank1rice/>
- [37] J. E. Gentle, *Matrix algebra: theory, computations, and applications in statistics*. Springer, 2007.
- [38] F. W. J. Olver, D. W. Lozier, R. F. Boisvert, and C. W. Clark, Eds., *NIST Handbook of Mathematical Functions*. Cambridge University Press, 2010. [Online]. Available: <http://dlmf.nist.gov/>
- [39] C. Siriteanu, S. Kuriki, D. Richards, and A. Takemura, “Chi-square mixture representations for the distribution of the scalar Schur complement in a noncentral Wishart matrix,” *Statistics and Probability Letters*, *accepted*, February 2016. [Online]. Available: <http://arxiv.org/abs/1512.08159>
- [40] M. Kang and M.-S. Alouini, “Largest eigenvalue of complex Wishart matrices and performance analysis of MIMO MRC systems,” *IEEE Journal on Selected Areas in Communications*, vol. 21, no. 3, pp. 418–426, 2003.
- [41] R. Chattamvelli, “A note on the noncentral-beta distribution,” *Amer. Statistician*, vol. 49, no. 2, pp. 231–234, 1995.